AFRL-SR-AR-TR-05-

0508

REPORT DOCUMENTATION PAGE

Public reporting burden for this collection of information is estimated to average 1 hour per response, including the time for reviewing inst
data needed, and completing and reviewing this collection of information. Send comments regarding this burden estimate or any other a
this burden to Department of Defense, Washington Headquarters Services, Directorate for Information Operations and Reports (0704-01
4302. Respondents should be aware that notwithstanding any other provision of law, no person shall be subject to any penalty for failing to comply with a collection of information if it does not display
valid OMB control number. **PLEASE DO NOT RETURN YOUR FORM TO THE ABOVE ADDRESS.**

1. REPORT DATE *(DD-MM-YYYY)*	2. REPORT TYPE	3. DATES COVERED *(From - To)*
17-11-2005	Final	Sep. 1, 03 - Nov. 17, 05

4. TITLE AND SUBTITLE
Development of a noise equivalent circuit model using experimental and numerical techniques

5a. CONTRACT NUMBER
F49620-03-1-0405

5b. GRANT NUMBER

5c. PROGRAM ELEMENT NUMBER

6. AUTHOR(S)
Kevin J. Webb

5d. PROJECT NUMBER

5e. TASK NUMBER

5f. WORK UNIT NUMBER

7. PERFORMING ORGANIZATION NAME(S) AND ADDRESS(ES)
School of Electrical and Computer Engineering
Purdue University
West Lafayette, IN 47907

VE

8. PERFORMING ORGANIZATION REPORT NUMBER

9. SPONSORING / MONITORING AGENCY NAME(S) AND ADDRESS(ES)
Dr. Gerald Witt
Program Manager, Phys. & Electr.
AFOSR
4015 Wilson Blvd., Room 713
Arlington, VA 22203

10. SPONSOR/MONITOR'S ACRONYM(S)

11. SPONSOR/MONITOR'S REPORT NUMBER(S)

12. DISTRIBUTION / AVAILABILITY STATEMENT
Distribution Statement A: unlimited

13. SUPPLEMENTARY NOTES

14. ABSTRACT
Noise equivalent circuit models in gallium nitride high electron mobility transistors have been developed using both experimental and numerical approaches. This work serves two primary purposes, to guide device development by establishing the primary causes for noise, and as a basis for models that will be used in transmitter and receiver design. The results of this work are applicable to noise mechanisms in other materials and devices.

15. SUBJECT TERMS
Transistor noise, models, measurements, GaN HEMTs

16. SECURITY CLASSIFICATION OF:			17. LIMITATION OF ABSTRACT	18. NUMBER OF PAGES	19a. NAME OF RESPONSIBLE PERSON
a. REPORT	b. ABSTRACT	c. THIS PAGE			19b. TELEPHONE NUMBER *(include area code)*

DISTRIBUTION STATEMENT A
Approved for Public Release
Distribution Unlimited

Final Report for F49620-03-1-0405

Development of a Noise Intrinsic Equivalent Circuit Model using Experimental and Numerical Techniques

Kevin J. Webb
School of Electrical and Computer Engineering,
Purdue University,
West Lafayette, IN 47907
webb@purdue.edu
Ph: 765-494-3373, Fax: 765-494-2706
Project Manager:
Gerald L. Witt
Physics and Electronics
Air Force Office of Scientific Research
gerald.witt@afosr.af.mil

November 17, 2005

1 Abstract

Noise equivalent circuit models in GaN HEMTs have been developed using both experimental and numerical approaches. This work serves two primary purposes, to guide device development by establishing the primary causes for noise, and as a basis for models that will be used in transmitter and receiver design. The results of this work will benefit the study of noise mechanisms in other materials and devices.

A nonlinear field effect transistor equivalent circuit model is examined to identify the fundamental mechanisms that up-convert baseband $1/f$ noise to near-carrier sideband noise when the device is operated in the large-signal regime. This model captures all physical noise sources and nonlinearities in the transistor, and thereby allows a general cause and effect treatment. The noise sources in the equivalent circuit model are determined using low-frequency spectrum analyzer and microwave noise figure-meter data. Using the example of an AlGaN/GaN high electron mobility transistor, the developed model correctly describes both the measured near-carrier sideband amplitude and phase noise simultaneously.

A numerical approach to simulate the intrinsic noise sources within transistors is described, and the impact of spatial correlation between local fluctuations is investigated. Using a two-dimensional numerical device solver, spectral densities for the gate and drain noise current sources and their correlation are evaluated using a Green's function approach, an equivalent of Shockley's impedance field method. Case studies with an AlGaN/GaN high electron mobility transistor are supported by measurement data. While local velocity fluctuations are correlated, the assumption of using uncorrelated diffusion noise source is found to be valid for the FET geometry studied.

20051215 159

2 Background

Wide bandgap aluminum gallium nitride/gallium nitride (AlGaN/GaN) high electron mobility transistors (HEMTs) have received much attention for high frequency, high power and high temperature operation, due to their high saturated electron drift velocity (1.3×10^7 cm/s), large breakdown field ($E_C > 3$ MV/cm), and good thermal conductivity, particularly with SiC substrates ($\theta \geq 3.3$ W/°K-cm) [1]. Furthermore, the high speed performance of AlGaN/GaN HEMTs can result in low microwave noise characteristics, making these devices candidates for receivers with a higher breakdown-related receiver damage threshold. For example, minimum microwave noise figures of 0.53 dB at 8 GHz (100 GHz f_T device, $V_{ds} = 8$ V) and 0.4 dB at 5 GHz (58 GHz f_T device, $V_{ds} = 1$ V) have been reported for AlGaN/GaN HEMTs [2, 3]. In the case of transmitter oscillators, low $1/f$ (or flicker) noise is important because the nonlinear up-conversion of $1/f$ noise into carrier sideband noise degrades the system performance. This low frequency $1/f$-type noise in AlGaN/GaN HEMTs has been associated with contributions from the traps [4, 5, 6].

Establishing a noise equivalent circuit model permits extraction of the intrinsic noise properties of AlGaN/GaN HEMTs, allowing performance prediction and study of noise mechanisms within the device. This model could then allow the prediction of oscillator phase noise, receiver noise, and the influence of physical effects such as traps and contacts. Furthermore, having a good noise model is critical for circuit design.

Noise models can be broadly classified into numerical and experimental approaches, both of which could lead to an equivalent circuit representation with adequate parameterization. Monte Carlo numerical studies can lead to port noise [7, 8]. A more tractable Green's function approach based on the transfer impedance concept of Shockley [9] has been applied [10]. The experimental two-port characterization yields three noise parameters, the minimum noise figure (F_{min}), the noise resistance (R_n, or conductance G_n), and the optimum source admittance for minimum noise ($Y_{opt} = G_{opt} + jB_{opt}$) [11]. With scattering (S)-parameter measurements, these measured noise parameters can be coupled to an equivalent circuit model, an approach that is common for microwave devices (see, for example, our previous work with noise in resonant tunneling diodes [12]).

Figure 1(a) shows the three physical sources of intrinsic device noise, where noise due to contacts and parasitics is excluded. The velocity fluctuation noise due to electron scatter in the channel is independent of frequency through the microwave frequency range of interest. The gate leakage current produces shot noise that can also be considered frequency independent. Finally, the capture and emission by interface and surface traps produces the $1/f$ noise. All these sources of noise can be folded into the Gaussian noise sources i_g and i_d in the FET equivalent circuit of Fig. 1(b), permitting a frequency-dependent representation of total intrinsic noise (and with the parasitic elements, the total extrinsic noise).

There has been an evolution of approaches to develop insight into the physics and circuit elements in Fig. 1. An empirical relation between the noise figure and the circuit parameters employing fitting parameters was proposed for GaAs FETs by Fukui [13]. More quantitative equivalent circuit modeling has been pursued by Statz *et al.* [14] and Pospieszalski [15], where the noise was represented equivalently as gate and drain temperature or resistance/conductance using Nyquist noise sources. In the case of the fundamental noise due to velocity fluctuations of the electrons in the channel, one would anticipate correlation between these gate and drain noise sources. The extraction of this correlation, necessary for the complete frequency dependent model, has received little attention. It has, however, been predicted numerically [10]. While the correlation was incorporated into the convenient extraction model proposed by Pucel *et al.* [16], it was not specifically studied. In other experimental work where the correlation was specifically addressed, it has not been treated rigorously as a free variable [15, 17, 18]. Thus far, noise equivalent circuit

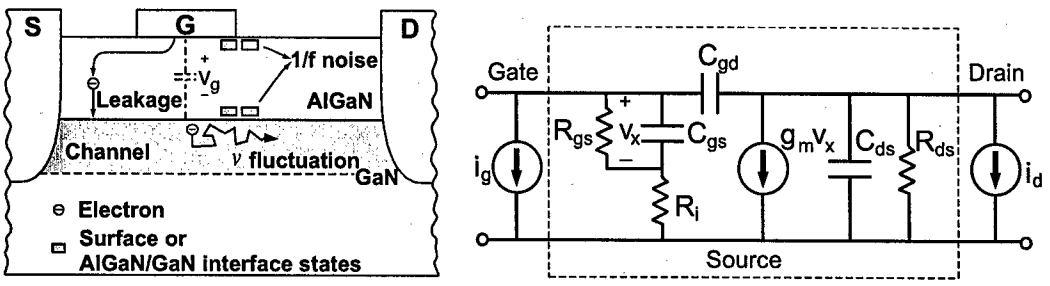

(a) (b)

Figure 1: (a) Fundamental noise mechanisms in AlGaN/GaN HEMTs. (b) Intrinsic noise equivalent circuit model with i_g and i_d representing partially correlated intrinsic noise sources. Inside the dashed box is now a noiseless two-port intrinsic transistor, and v_x is the deterministic drive signal.

models for GaN HEMTs have received little attention [3, 19, 20, 21].

The features of GaN HEMTs make them good candidates as sources, i.e., for use in microwave oscillators, an essential component in an RF communication system. Intentionally unstable, oscillators are triggered by transients or noise, and the amplitude of oscillation increases due to device nonlinearities until it reaches a stable state with self-limited amplitude. Under large signal operation in an oscillator, the active device nonlinearities result in the up-conversion of the low frequency noise, which gives rise to noise sidebands around the oscillation frequency in the spectrum, thus degrading the spectral purity of the oscillator. An equivalent circuit model therefore needs to contain suitable element nonlinearities.

3 Noise in Transistors Under Nonlinear Operating Conditions

A transistor operated under large-signal conditions up-converts the intrinsic $1/f$ noise into amplitude-modulated and phase-modulated sidebands (amplitude and phase noise) around the carrier, and these can be discriminated in a measurement. For example, in GaAs transistors, the measured amplitude and phase noise levels have been found comparable [22]. Therefore, a complete large-signal noise equivalent circuit should correctly describe both amplitude and phase noise. Oscillator amplitude noise is typically much smaller than the oscillator phase noise, due to the self-amplitude-limiting mechanism [23]. As a consequence, there have been major efforts over a long time period to understand the dominant phase noise in transistor-based oscillators (see, for example, [24, 25, 26, 27, 28]).

A measurement-based nonlinear noise equivalent-circuit model allows study of fundamental mechanisms which will up-convert the baseband $1/f$ noise to the near-carrier sideband noise. To produce this model, the linear and nonlinear equivalent circuit elements need to be determined, as well as the noise sources, i.e., the baseband $1/f$ noise needs to be measured. Driving the transistor in an amplifier configuration, rather than as an oscillator, allows for precise control over the operating conditions, facilitating parameterization of a nonlinear device noise model [29, 30, 31, 32]. The resulting nonlinear transistor model, configured as an amplifier, has been treated using harmonic balance simulation, where the coefficients in a finite Fourier expansion of voltage or current are determined numerically. This type of analysis has been used to relate a nonlinear model to amplitude noise [31] and to phase noise [29, 30]. The impact of transistor nonlinearities

on the baseband noise up-conversion have been investigated through an analytic study of FET oscillators [33, 34]. The general understanding that has evolved is that in field effect transistors (FETs), the nonlinear gate-source capacitance (C_{gs}) gives rise to phase noise and the nonlinear transconductance (g_m) and, to a lesser degree, the output conductance (g_{ds}), contribute to the amplitude noise [34]. This view has led to simplified nonlinear noise equivalent circuits, and has also led to the use of only a gate equivalent noise source [34]. In reality, and as we show, this delineation of the noise source contributions is not possible in general. Furthermore, it is necessary to consider both noise sources at the input and the output.

We developed a measurement-based large-signal noise equivalent-circuit transistor model which includes all physical noise sources, and applied this model to an AlGaN/GaN high electron mobility transistor (HEMT). This model correctly describes both amplitude and phase noise in the transistor. The major noise sources and nonlinearities are captured in a simplified analytic model, thereby allowing a conceptual theory to be developed. These models allow the fundamental understanding of how the near-carrier amplitude and phase noise sidebands are generated when the device is operated in the large-signal regime. The AlGaN/GaN HEMT used for this study was grown on a SiC substrate and processed as described elsewhere [1]. The HEMT has significant $1/f$ noise that will form the dominant sideband noise in a nonlinear amplifier or an oscillator.

The emphasis of this study was to establish the precise relation between the intrinsic noise sources and the near-carrier sideband noise in terms of the transistor nonlinearities. A simplified analytical model for the in-phase amplitude noise and the quadrature phase noise provides the qualitative picture, which has been supported with a more general nonlinear model, that the amplitude noise is dominated by the nonlinear transconductance and the phase noise has important contribution from the gate capacitance nonlinearity as well as the nonlinear transconductance. As the gate parasitic resistance provides the vehicle that produces that phase noise, one can expect that reducing the gate contact resistance will have significant impact on oscillator noise performance. Both the input and output noise sources appear significant and should be incorporated into nonlinear device noise models. Although the nonlinear model was validated only for an AlGaN/GaN HEMT, it appears that this view should be applicable to all FETs. The example large signal model used works effectively, and allowed the impact of physical noise sources and nonlinearities to be evaluated. It should be able to accurately model FETs during the design of, for example, oscillators.

The results of this work were presented at the 2004 IEEE International Microwave Symposium [32], and a journal paper has appeared in the IEEE Transactions on Microwave Theory and Techniques [35]. This journal paper is included in the Appendix of this report.

4 Numerical Noise Model

More complete interrogation of the device noise can be established using numerical models for the noise sources. The impedance field method for numerical transistor noise modeling, first proposed by Shockley [9], involves the determination of the Green's function (or impedance field), i.e., the influence of a local fluctuation (in terms of current or voltage at one point in the channel) at the gate and drain terminals, in the case of the field-effect transistor (FET). This method has enabled the intrinsic noise sources (gate and drain noise sources and their correlation) to be determined [10, 36].

In the impedance field method, the channel is divided into many voxels for numerical simulation. For long channel devices, the volume of each voxel can be sufficiently large so that local velocity fluctuations can be assumed to be spatially uncorrelated between voxels. This assumption of uncorrelated noise sources has been commonly used to simplify the problem and to calculate the

intrinsic noise sources [9, 10, 37]. However, as the device and voxel size shrinks, local noise sources (due to velocity fluctuation) between voxels can be correlated because a significant number of electrons can travel between nearby voxels without their velocity being randomized significantly.

The spatial correlation between local velocity fluctuations has been studied numerically. The two-point cross-correlation function of velocities at different spatial positions can be related to the probability that electrons travel between points without their velocity being randomized by scattering events [38]. With a Monte-Carlo simulation, the cross-correlation function of the velocity fluctuations in different segments inside a one-dimensional (1-D) GaAs structure was obtained by tracking the kinetics of individual electrons within the device [39, 40]. This demonstrated the practical importance of retaining correlations between the noise sources in neighboring voxels.

We have used a two-dimensional (2-D) numerical approach to investigate the effect of spatially correlated local noise sources on the gate and drain terminal noise in the FET geometry. While Monte-Carlo simulation can determine the numerical values of the spatially correlated local noise sources [39], it is computationally inefficient. Our proposed approach is in the framework of the drift-diffusion model that we find valid for noise modeling even for the sub-micron gate length device considered. Using this model, diffusion noise sources and Green's functions are determined. We assume that the independent (uncorrelated) local diffusion noise sources that are initially obtained from the drift-diffusion model are, in fact, comprised of contributions from correlated noise terms involving the nearby voxels. Then, the coupling of the local noise sources (either correlated or uncorrelated) to the gate and drain terminal in the FET is simulated using the Green's function approach to study the merit of assuming spatially correlated noise sources. We use the example of an aluminum gallium-nitride/gallium-nitride high electron mobility transistor (AlGaN/GaN HEMT) that was fabricated as part of a program to develop high power microwave sources and amplifiers [1]. The high mobility in the 2-D electron gas (2DEG) not only results in high operating frequencies, but also low microwave noise, making AlGaN/GaN HEMTs suitable for low noise receivers, hence the interest in their microwave noise properties [41].

In the 0.25 μm AlGaN/GaN HEMT studied, the correlation of the diffusion noise source over meaningful lengths did not alter the terminal noise significantly, leading to the conclusion that an uncorrelated model is sufficient. One would expect that for yet smaller device geometries noise source correlation would become more important. Such smaller-scale devices may require a Boltzmann transport equation model. It is possible that there is a regime where a drift-diffusion noise model is applicable and correlation is important, making the simple neighborhood correlation concept introduced an expedient tool. While the numerical implementation described involved a drift-diffusion model to determine both the noise sources and the Green's functions, the concept of noise sources based on velocity fluctuations is general, as is the notion of a neighborhood correlation scheme.

A paper on this numerical noise model was presented at the 2004 IEEE International Microwave Symposium [42], and a journal paper was submitted to the IEEE Transactions on Electron Devices (see the Appendix) [43], which has now been revised based on the reviewers' suggestions.

References

[1] L. F. Eastman, V. Tilak, J. Smart, B. M. Green, E. M. Chumbes, R. Dimitrov, H. Kim, O. S. Ambacher, N. Weimann, T. Prunty, M. Murphy, W. J. Schaff, and J. R. Shealy, "Undoped AlGaN/GaN HEMTs for microwave power amplification," *IEEE Trans. Electron Devices*, vol. 48, no. 3, pp. 479–485, Mar. 2001.

[2] W. Lu, J. Yang, M. A. Khan, and I. Adesida, "AlGaN/GaN HEMT's on SiC with over 100 GHz f_T and low microwave noise," *IEEE Trans. Electron Devices*, vol. 48, no. 3, pp. 581–585, Mar. 2001.

[3] T. Hussain, A. Kurdoghlian, P. Hashimoto, W. S. Wong, M. Wetzel, J. S. Moon, L. McCray, and M. Micovic, "GaN HFETs with excellent low noise performance at lower power levels through the use of thin AlGaN Schottky barrier layer," in *International Electron Devices Meeting Technical Digest*, 2001, pp. 581–584.

[4] W. Y. Ho, C. Surya, K. Y. Tong, W. Kim, A. E. Botcharev, and H. Morkoc, "Characterization of flicker noise GaN-based MODFET's at low drain bias," *IEEE Trans. Electron Devices*, vol. 46, no. 6, pp. 1099–1104, June 1999.

[5] A. Balandin, S. V. Morozov, S. Cai, R. Li, K. L. Wang, G. Wijeratne, and C. R. Viswanathan, "Low flicker noise GaN/AlGaN heterostructure field effect transistors for microwave communications," *IEEE Trans. Microwave Theory Tech.*, vol. 47, no. 8, pp. 1413–1417, Aug. 1999.

[6] S. L. Rumyantsev, N. Pala, M. S. Shur, E. Borovitskaya, A. P. Dmitriev, M. E. Levinshtein, R. Gaska, M. A. Khan, J. Yang, X. Hu, and G. Simin, "Generation-recombination noise in GaN/AlGaN heterostructure field effect transistors," *IEEE Trans. Electron Devices*, vol. 48, no. 3, pp. 530–534, Mar. 2001.

[7] C. Moglestue, "A Monte Carlo study of the intrinsic noise figure in GaAs MESFET's," *IEEE Trans. Electron Dev.*, vol. 32, no. 12, pp. 2092–2096, Dec. 1985.

[8] J. Mateos, T. Gonzalez, D. Pardo, V. Hoel, and A. Cappy, "Monte Carlo simulator for the design optimization of low-noise HEMTs," *IEEE Trans. Electron Dev.*, vol. 47, no. 10, pp. 1950–1956, Oct. 2000.

[9] W. Shockley, J. A. Copeland, and R. P. James, "The impedance field method of noise calculation in active semiconductor devices," in *Quantum Theory of Atoms, Molecules, and the Solid State*, 1966, pp. 537–563, New York: Academic Press.

[10] A. Cappy, "Noise modeling and measurement techniques," *IEEE Trans. Microwave Theory Tech.*, vol. 36, no. 1, pp. 1–10, Jan. 1988.

[11] H. Rothe and W. Dahlke, "Theory of noisy fourpoles," *Proc. IRE*, vol. 44, pp. 811–818, June 1956.

[12] A. Przadka, K. J. Webb, and D. B. Janes, "Two-port noise and impedance measurements for two-terminal devices with a resonant tunneling diode example," *IEEE Trans. Microwave Theory Tech.*, vol. 46, no. 9, pp. 1215–1220, Sep. 1998.

[13] H. Fukui, "The noise performance of microwave transistors," *IEEE Trans. Electron Devices*, vol. 13, pp. 329–341, Mar. 1966.

[14] H. Statz, H. A. Haus, and R. A. Pucel, "Noise characteristics of gallium arsenide field-effect transistors," *IEEE Trans. Electron Devices*, vol. 21, pp. 549–562, Sep. 1974.

[15] M. W. Pospieszalski, "Modeling of noise paramters of MESFET's and MODFET's and their frequency and temperature dependence," *IEEE Trans. Microwave Theory Tech.*, vol. 36, no. 1, pp. 1–10, Jan. 1988.

[16] R. A. Pucel, W. Struble, R. Hallgren, and U. L. Rohde, "A general noise de-embedding procedure for packaged two-port linear active devices," *IEEE Trans. Microwave Theory Tech.*, vol. 40, no. 11, pp. 2013–2024, Nov. 1992.

[17] P. Heymann, M. Rudolph, H. Prinzler, R. Doerner, L. Klapproth, and G. Bock, "Experimental evaluation of microwave field-effect-transistor noise models," *IEEE Trans. Microwave Theory Tech.*, vol. 47, no. 2, pp. 156–163, Feb. 1999.

[18] J. Stenarson, M. Garcia, I. Angelov, and H. Zirath, "A general parameter-extraction method for transistor noise models," *IEEE Trans. Microwave Theory Tech.*, vol. 47, no. 12, pp. 2358–2363, Dec. 1999.

[19] S. Lee, V. Tilak, K. J. Webb, and L. F. Eastman, "Intrinsic noise characteristics of AlGaN/GaN HEMTs," in *2002 IEEE MTT-S Int. Microwave Symp. Dig.*, June 2002, vol. 3, pp. 1415–1418, Seattle, WA.

[20] S. Lee, K. J. Webb, V. Tilak, and L. F. Eastman, "Intrinsic AlGaN/GaN HEMT noise from a measurement-based equivalent circuit model," in *Device Research Conference Digest (Late news)*, June 2002, Santa Barbara, CA.

[21] S. Lee, K. J. Webb, V. Tilak, and L. F. Eastman, "Intrinsic noise equivalent circuit parameters for AlGaN/GaN HEMTs," *IEEE Trans. Microwave Theory Tech.*, vol. 51, no. 5, pp. 1567–1577, May 2003.

[22] P. A. Dallas and J. K. A. Everard, "Characterization of flicker noise in GaAs MESFET's for oscillator applications," *IEEE Trans. Microwave Theory Tech.*, vol. 48, no. 2, pp. 245–257, Feb. 2000.

[23] M. N. Tutt, D. Pavlidis, A. Khatibzadeh, and B. Bayraktaroglu, "The role of baseband noise and its upconversion in HBT oscillator phase noise," *IEEE Trans. Microwave Theory Tech.*, vol. 43, no. 7, pp. 1461–1471, July 1995.

[24] D. B. Leeson, "A simple model of feedback oscillator noise spectrum," *Proc. IEEE*, vol. 54, no. 2, pp. 329–330, Feb. 1966.

[25] R. A. Pucel and J. Curtis, "Near-carrier noise in FET oscillators," in *1983 IEEE MTT-S Int. Microwave Symp. Dig.*, 1983, pp. 284–284.

[26] J. Verdier, O. Llopis, R. Plana, and J. Graffeuil, "Analysis of noise up-conversion in microwave field-effect transistor oscillators," *IEEE Trans. Microwave Theory Tech.*, vol. 44, no. 8, pp. 1478–1483, Aug. 1996.

[27] T. H. Lee and A. Hajimiri, "Oscillator phase noise: a tutorial," *IEEE J. Solid-State Circuits*, vol. 35, no. 3, pp. 326–336, Mar. 2000.

[28] A. Laloue, A. Lyoubi, M. Camiade, J. C. Nallatamby, M. Valenza, M. Prigent, and J. Obregon, "A measurement based distributed low frequency noise HEMT model: application to design of millimeter wave automotive radar chip sets," in *2001 IEEE MTT-S Int. Microwave Symp. Dig.*, May 2001, pp. 423–426, Phoenix, AZ.

[29] O. Llopis, J. B. Juraver, B. Tamen, F. Danneville, M. Chaubet, A. Cappy, and J. Graffeuil, "Nonlinear noise modeling of a PHEMT device through residual phase noise and low frequency

noise measurements," in *2001 IEEE MTT-S Int. Microwave Symp. Dig.*, May 2001, pp. 831–834, Phoenix, AZ.

[30] G. Cibiel, M. Regis, O. Llopis, A. Rennane, L. Bary, R. Plana, Y. Kersale, and V. Giordano, "Optimization of an unltra low-phase noise sapphier-SiGe HBT oscillator using nonlinear CAD," *IEEE Trans. Ultrasonics, Ferroelectrics, Frequency Control*, vol. 51, no. 1, pp. 33–41, Jan. 2004.

[31] D. R. Pehlke, A. Sailer, W. J. Ho, J. A. Higgins, H. Smith, J. Hebert, and M. Vineyard, "A predictive model describing the upconversion of 1/f noise into AM sidebnad noise in HBTs," in *Device Research Conference Digest*, 1995, pp. 94–95.

[32] S. Lee, K. J. Webb, and L. F. Eastman, "The influence of transistor nonlinearities on intrinsic noise," in *2004 IEEE MTT-S Int. Microwave Symp. Dig.*, June 2004, Fort Worth, TX.

[33] B. T. Debney and J. S. Joshi, "A theory of noise in GaAs FET microwave oscillators and its experimental verification," *IEEE Trans. Electron Dev.*, vol. 30, no. 7, pp. 769–772, July 1983.

[34] H. J. Siweris and B. Schiek, "Analysis of noise upconversion in microwave FET oscillators," *IEEE Trans. Microwave Theory Tech.*, vol. 33, no. 3, pp. 233–242, Mar. 1985.

[35] S. Lee and K. J. Webb, "The influence of transistor nonlinearities on noise properties," *IEEE Trans. Microwave Theory Tech.*, vol. 53, no. 4, pp. 1314–1321, Apr. 2005.

[36] F. Bonani and G. Ghione, *Noise in Semiconductor Devices*, Springer-Verlag, 2001.

[37] J. P. Nougier, "Fluctuations and noise of hot carriers in semiconductor materials and devices," *IEEE Trans. Electron Dev.*, vol. 41, no. 11, pp. 2034–2048, Nov. 1994.

[38] J. P. Nougier, J. C. Vaissiere, and C. Gontrand, "Two-point correlations of diffusion noise sources of hot carriers in semiconductors," *Phys. Rev. Lett.*, vol. 51, no. 6, pp. 513–516, Aug. 1983.

[39] J. Mateos, T. Gonzalez, and D. Pardo, "Spatial extent of the correlations between local diffusion noise sources in GaAs," *J. Appl. Phys.*, vol. 77, no. 4, pp. 1564–1568, Feb. 1995.

[40] J. Mateos, T. Gonzalez, and D. Pardo, "Influence of spatial correlations on the analysis of diffusion noise in submicron semiconductor structures," *Appl. Phys. Lett.*, vol. 67, no. 5, pp. 685–687, July 1995.

[41] P. B. Shah, D. D. Smith, T. E. Griffin, K. A. Jones, and S. T. Sheppard, "Carrier transport related analysis of high-power AlGaN/GaN HEMT structures," *IEEE Trans. Electron Devices*, vol. 47, no. 3, pp. 308–312, Feb. /2000.

[42] S. Lee and K. J. Webb, "Numerical noise model for the AlGaN/GaN HEMT," in *2004 IEEE MTT-S Int. Microwave Symp. Dig.*, June 2004, Fort Worth, TX.

[43] S. Lee and K. J. Webb, "A correlated diffusion noise model for the field-effect transistor," *IEEE Trans. Electron. Dev.*

Appendix: Journal Papers

The Influence of Transistor Nonlinearities on Noise Properties

Sungjae Lee, *Member, IEEE,* and Kevin J. Webb, *Fellow, IEEE*

***Abstract*—A nonlinear field-effect transistor equivalent-circuit model is examined to identify the fundamental mechanisms that up-convert baseband $1/f$ noise to near-carrier sideband noise when the device is operated in the large-signal regime. This model captures all physical noise sources and nonlinearities in the transistor, and thereby allows a general cause-and-effect treatment. The noise sources in the equivalent-circuit model are determined using low-frequency spectrum analyzer and microwave noise-figure meter data. Using the example of an AlGaN/GaN high electron-mobility transistor, the developed model correctly describes both the measured near-carrier sideband amplitude and phase noise simultaneously.**

***Index Terms*—Amplitude noise, gallium nitride, noise measurement, nonlinearities, phase noise, semiconductor device noise.**

I. Introduction

TRANSMITTER or oscillator noise is constituted by noise sidebands modulating a carrier. In the case of transistors, this sideband noise is primarily attributed to baseband $1/f$ noise, which is mixed up to the microwave carrier frequency due to transistor nonlinearities. This near-carrier sideband noise limits system performance because it degrades the signal-to-noise ratio for the near-carrier signals.

A transistor operated under large-signal conditions up-converts the intrinsic $1/f$ noise into amplitude- and phase-modulated sidebands (amplitude and phase noise) around the carrier, and these can be discriminated in a measurement. For example, in GaAs transistors, the measured amplitude and phase-noise levels have been found comparable [1]. Therefore, a complete large-signal noise equivalent circuit should correctly describe both amplitude and phase noise. Oscillator amplitude noise is typically much smaller than the oscillator phase noise due to the self-amplitude-limiting mechanism [2]. As a consequence, there have been major efforts over a long time period to understand the dominant phase noise in transistor-based oscillators (see, e.g., [3]–[7]).

A measurement-based nonlinear noise equivalent-circuit model allows study of fundamental mechanisms which will up-convert the baseband $1/f$ noise to the near-carrier sideband noise. To produce this model, the linear and nonlinear equivalent-circuit elements need to be determined, as well as the noise sources, i.e., the baseband $1/f$ noise needs to be measured. Driving the transistor in an amplifier configuration, rather than as an oscillator, allows for precise control over the operating conditions, facilitating parameterization of a nonlinear device noise model [8]–[11]. The resulting nonlinear transistor model, configured as an amplifier, has been treated using harmonic-balance simulation, where the coefficients in a finite Fourier expansion of voltage or current are determined numerically. This type of analysis has been used to relate a nonlinear model to amplitude noise [10] and to phase noise [8], [9]. The impact of transistor nonlinearities on the baseband noise up-conversion have been investigated through an analytic study of field-effect transistor (FET) oscillators [12], [13]. The general understanding that has evolved is that, in FETs, the nonlinear gate–source capacitance ($C_{\rm gs}$) gives rise to phase noise and nonlinear transconductance (g_m) and, to a lesser degree, the output conductance ($g_{\rm ds}$), contribute to the amplitude noise [13]. This view has led to simplified nonlinear noise equivalent circuits, and has also led to the use of only a gate equivalent noise source [13]. In reality, and as we show, this delineation of the noise source contributions is not, in general, possible. Furthermore, it is necessary to consider both noise sources at the input and output.

We present an example measurement-based large-signal noise equivalent-circuit transistor model, which includes all physical noise sources, and apply this model to an AlGaN/GaN high electron-mobility transistor (HEMT). This model correctly describes both amplitude and phase noise in the transistor. The major noise sources and nonlinearities are captured in a simplified analytic model, thereby allowing a conceptual theory to be developed. These models allow the fundamental understanding of how the near-carrier amplitude and phase-noise sidebands are generated when the device is operated in the large-signal regime. The AlGaN/GaN HEMT used for this study was grown on an SiC substrate and processed as described elsewhere [14]. The HEMT has significant $1/f$ noise that will form the dominant sideband noise in a nonlinear amplifier or an oscillator.

Section II describes an underlying noise theory using a simplified model that is subsequently related to the more general transistor nonlinear model of Section III. Noise sideband measurements and model predictions for the GaN HEMT are presented in Section IV.

Manuscript received May 27, 2004; revised September 16, 2004. This work was supported by the Air Force Office of Scientific Research under Contract F49620-03-1-0405 and by the Office of Naval Research under Contract N00014-99-C-0172.

S. Lee was with the School of Electrical and Computer Engineering, Purdue University, West Lafayette, IN 47907 USA. He is now with IBM Microelectronics, Essex Junction, VT 05452 USA.

K. J. Webb is with the School of Electrical and Computer Engineering, Purdue University, West Lafayette, IN 47907 USA (e-mail: webb@purdue.edu).

Digital Object Identifier 10.1109/TMTT.2005.845763

0018-9480/$20.00 © 2005 IEEE

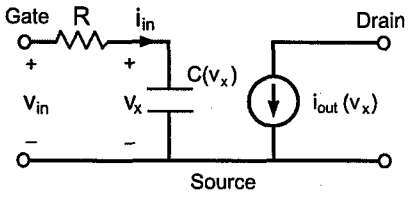

Fig. 1. Nonlinear transistor equivalent circuit with capacitor and transconductance nonlinearities.

II. Nonlinear Transistor Noise Theory

A. Simplified Nonlinear Transistor Model

In the case of a nonlinear FET, and considering the simple model of Fig. 1 (with ac signals only), the voltage-dependent input and output ac currents can be represented by a Taylor-series expansion. Assuming weak or moderate nonlinearities and, hence, terms up to second order,

$$i_{\text{in}}(t) = C_1 \frac{dv_x(t)}{dt} + C_2 v_x(t) \frac{dv_x(t)}{dt} \tag{1}$$

$$i_{\text{out}}(t) = g_{m1} v_x(t) + g_{m2} v_x^2(t) \tag{2}$$

where v_x is the ac voltage across the input capacitance, C_1 and g_{m1} are the linear capacitance and transconductance, and C_2 (F/V) and g_{m2} (A/V^2) represent the capacitance and transconductance nonlinearities, respectively. Equations (1) and (2) are coupled, as both i_{in} and i_{out} are a function of v_x. Using $v_{\text{in}}(t) = Ri_{\text{in}}(t) + v_x(t)$ with (1) leads to

$$v_{\text{in}}(t) = RC_1 \frac{dv_x(t)}{dt} + RC_2 v_x(t) \frac{dv_x(t)}{dt} + v_x(t) \tag{3}$$

a nonlinear differential equation in v_x. Note that, in this simple model, the linear series resistor R is an important contributor to the nonlinear capacitance terms. If $R = 0$ in (3), $v_{\text{in}}(t) = v_x(t)$, and the capacitive nonlinearity will not have an impact on the output current i_{out}. The series resistor R may correspond to the parasitic resistance (due to the FET gate metal) or the channel resistance in the complete equivalent-circuit model.

Note that a second-order series expansion for both i_{in} and i_{out} is used in our simplified conceptual model, which allows a cause-and-effect treatment to provide analytical insight. Later, we present a higher order model for an AlGaN/GaN HEMT equivalent circuit, thus allowing for more accurate simulation, and we compare the harmonic-balance simulation results for this model with the measurement data. In the actual simulation and measurement, the transistor amplifier (i.e., the AlGaN/GaN HEMT) is driven by the input source to operate in the weakly (or moderately) nonlinear regime. Therefore, the second-order nonlinearity terms in the model dominate those from higher order nonlinearities, allowing application of the simple model we presented here. Note that, in the oscillator application, third-order and higher order terms are no longer negligible, as the transistor is typically operated in a strongly nonlinear regime. While our analytic approach assumes a nonlinear model with terms only up to second order to investigate the up-conversion mechanism, it provides a basis that can be generalized to the higher order model we use for the AlGaN/GaN HEMT that can be applied in specific applications.

Consider that $v_{\text{in}}(t) = v(t)$, where $v(t)$ is a deterministic sinusoidal signal given by

$$v(t) = V_p \cos(\omega_0 t) \tag{4}$$

where ω_0 is the angular frequency $2\pi f_0$. The solution of (3) for $v_x(t)$ then requires harmonics of the excitation frequency ω_0. While the excitation signal is an even function in time (cosine), the resulting harmonics from (3) for $v_x(t)$ should have both cosine (even) and sine (odd) terms due to the capacitive nonlinearity. Therefore, we assume the finite Fourier series expansion

$$\begin{aligned} v_x(t) &= a_0 + \sum_{n=1}^{N} a_n \cos(n\omega_0 t) + b_n \sin(n\omega_0 t) \\ &= c_0 + \sum_{n=1}^{N} c_n e^{jn\omega_0 t} + c_n^* e^{-jn\omega_0 t} \end{aligned} \tag{5}$$

where a_n and b_n are the Fourier coefficients of $v_x(t)$ and $c_0 = a_0$, and the complex Fourier coefficient $c_n = (1/2)(a_n - jb_n)$. The complex series form simplifies the calculation. Using $N = 2$ in (5) as an approximation to $v_x(t)$, substituting it into (3), and equating terms up to second order, we obtain

$$c_0 = 0 \tag{6}$$

$$c_1 \simeq \frac{V_p}{2} \tag{7}$$

$$c_2 \simeq -j\omega_0 RC_2 \left(\frac{V_p}{2}\right)^2. \tag{8}$$

The approximations in (7) and (8) result from neglecting terms under the assumption that $\omega_0 RC_2 \ll \omega_0 RC_1 \ll 1$, which is the case for most FETs operating at microwave frequencies. Substituting (6)–(8) into (5) gives

$$\begin{aligned} v_x(t) &= V_p \cos(\omega_0 t) + \frac{V_p^2 \omega_0 RC_2}{2} \sin(2\omega_0 t) \\ &= V_p \cos(\omega_0 t) - RC_2 V_p \cos(\omega_0 t) \frac{d\left(V_p \cos(\omega_0 t)\right)}{dt}. \end{aligned} \tag{9}$$

Finally, using (4), (9) can be rewritten as

$$v_x(t) = v_{\text{in}}(t) - RC_2 v_{\text{in}}(t) \frac{dv_{\text{in}}(t)}{dt}. \tag{10}$$

Applying (10) to (2) gives

$$\begin{aligned} i_{\text{out}}(t) &= g_{m1} v_{\text{in}}(t) + g_{m2} v_{\text{in}}^2(t) - g_{m1} RC_2 v_{\text{in}}(t) \frac{dv_{\text{in}}(t)}{dt} \\ &\quad - 2g_{m2} RC_2 v_{\text{in}}^2(t) \frac{dv_{\text{in}}(t)}{dt} \\ &\quad + g_{m2} R^2 C_2^2 v_{\text{in}}^2(t) \left(\frac{dv_{\text{in}}(t)}{dt}\right)^2 \end{aligned} \tag{11}$$

where $g_{m2} v_{\text{in}}^2(t)$ represents the memoryless nonlinearity in the transconductance, the third term on the right-hand side of (11) accounts for the capacitive nonlinearity (and, thus, the memory effect because the capacitor is a charge storage element), and the

last two terms represent coupled transconductance and capacitance nonlinearities. We note that the last two terms in (11) have not appeared in prior work (see, e.g., [13]) and that the fourth (second to last) term in (11) is necessary to explain our amplitude and phase-noise measurements.

B. Baseband Noise Up-Conversion

For the noise random process $n(t)$, we write the mean as $\langle n(t)\rangle$, where $\langle\rangle$ denotes the statistical average, the autocorrelation as $R_{nn}(t,\tau)$ $(= \langle n(t)n(t+\tau)\rangle)$, and the power spectral density as $\langle|n(\omega)|^2\rangle$. Here, $n(t)$ is either the voltage across or the current through a 1-Ω resistor, unless stated otherwise. Thus, regardless of whether $n(t)$ represents a voltage or current, the normalized power spectral density is expressed as $\langle|n(\omega)|^2\rangle$. We assume a zero-mean wide-sense stationary random process $n(t)$, a consequence of assuming band-limited noise, so that $R_{nn}(\tau)$ and $\langle|n(\omega)|^2\rangle$ form a Fourier transform pair [15]. This assumption is valid for trap-related $1/f$ noise sources (even with large-signal operation) because, physically, traps with a long time constant cannot follow the fast carrier signal and are only influenced by the average (dc bias).

Now, assume that $v_{\rm in}(t) = v(t) + n(t)$, where $n(t)$ is a voltage noise source at the input and $v(t)$ is given by (4). The nonlinear relation defined in (11) between $v_{\rm in}(t)$ and $i_{\rm out}(t)$ is invariant with the addition of the noise source [13]. The last term on the right-hand side of (11) is much smaller than the other terms and is, thus, ignored. The nonlinear terms (g_{m2}, C_2) in (11) generate additional baseband noise, and sideband noise near ω_0 and $2\omega_0$. We focus on the noise near ω_0, $n_0(t)$, which is given by

$$\begin{aligned} n_0(t) = {} & 2g_{m2}V_p\cos(\omega_0 t)n(t) \\ & + g_{m1}\omega_0 RC_2V_p\sin(\omega_0 t)n(t) \\ & + 2g_{m2}\omega_0 RC_2V_p\sin(\omega_0 t)n^2(t) \\ & - g_{m1}RC_2V_p\cos(\omega_0 t)\frac{dn(t)}{dt} \\ & - 4g_{m2}RC_2V_p\cos(\omega_0 t)\frac{dn(t)}{dt}n(t). \end{aligned} \tag{12}$$

Since $n_0(t)$ is narrow-band, it can be represented in terms of modulation sidebands as

$$n_0(t) = n_I(t)\cos(\omega_0 t) - n_Q(t)\sin(\omega_0 t) \tag{13}$$

where $n_I(t)$ is the in-phase (amplitude) noise component and $n_Q(t)$ is the quadrature (phase) noise component, both with respect to the carrier [16], [17]. From (12) and (13),

$$\begin{aligned} n_I(t) = {} & 2g_{m2}V_p n(t) - g_{m1}RC_2V_p\frac{dn(t)}{dt} \\ & - 4g_{m2}RC_2V_p\frac{dn(t)}{dt}n(t) \end{aligned} \tag{14}$$

$$n_Q(t) = -g_{m1}\omega_0 RC_2V_p n(t) - 2g_{m2}\omega_0 RC_2V_p n^2(t). \tag{15}$$

Equation (14) indicates that the amplitude noise results from both transconductance (g_{m2}) and capacitance (C_2) nonlinearities. From (15), the phase noise also depends on both capacitance and transconductance nonlinearities. If $g_{m1}RC_2 \ll g_{m2}$ and $RC_2 \ll 1$, the last two terms of (14) can be neglected. Our experimental data indeed indicates that the contribution from these terms to the overall amplitude noise is small, and that n_I can be reasonably well represented by the first term in (14). In contrast, our experiment indicates that both terms in (15) are important. In fact, the second term has the dominant influence. Note also that the modulation coefficient (the amount of up-conversion) depends not only on the transistor nonlinearities (g_{m2} and C_2), but also on the carrier power (through V_p) and carrier frequency (ω_0) in the case of the phase noise $n_Q(t)$. It is also worth noting in (14) and (15) that the capacitive nonlinearity (C_2) will not affect the phase noise if the series resistor (a linear element in this model) R is zero. The noise dependence on R suggests that, if the series resistance at the input can be lowered (e.g., the parasitic gate metal resistance), the near-carrier sideband noise, in particular the phase noise, would be reduced. Also, while there is negligible phase noise as $C_2 \to 0$, both amplitude and phase noise can remain as $g_{m2} \to 0$.

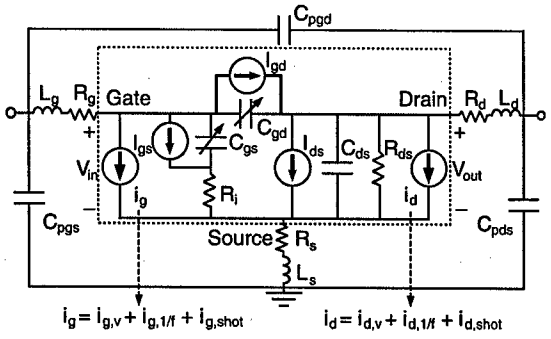

Fig. 2. Large-signal noise equivalent circuit. Inside the dotted box is the intrinsic device with intrinsic noise sources i_g and i_d. R_g, R_s, and R_d have extrinsic thermal noise, which are not shown.

III. Nonlinear Noise Equivalent Circuit

As an example of a nonlinear model, we apply the large-signal equivalent circuit of Fig. 2 that we have previously found suitable for the AlGaN/GaN HEMT used in our noise studies [18]. This model is based on that proposed by Curtice and Ettenberg [19] and uses a nonlinear description of the drain current, gate-to-source (and gate-to-drain) capacitance, and diode I–V characteristics ($I_{\rm gs}$ and $I_{\rm gd}$ in Fig. 2). Our prior work has validated this model based on comparisons with dc, S-parameter, and RF power sweep data [20]. The total (dc + ac) drain-to-source current is assumed to be

$$\begin{aligned} I_{\rm ds} = {} & \left(A_0 + A_1V_1 + A_2V_1^2 + A_3V_1^3\right) \\ & \cdot\tanh(\gamma V_{\rm out})(1+\lambda V_{\rm out}) \end{aligned} \tag{16}$$

where

$$V_1 = V_{\rm in}(t-\tau_t)\left(1+\beta(V_{\rm dso}-V_{\rm out})\right). \tag{17}$$

$V_{\rm in}(t)$ and $V_{\rm out}(t)$ are the gate-to-source and drain-to-source voltages (dc + ac), γ is the drain current saturation parameter, λ controls $I_{\rm ds}$ in the saturation region, τ_t is the electron transit time, β describes the pinchoff dependence on $V_{\rm out}$, and $V_{\rm dso}$ is

TABLE I
LARGE-SIGNAL EQUIVALENT-CIRCUIT PARAMETERS FOR THE 0.25 × 250 μm^2 ALGaN/GaN HEMT

A_0	A_1	A_2	A_3	γ	λ
0.1764	0.0154	-0.0091	-0.0010	0.7896	0.0524
β	τ_t	C_{gso}	C_{gdo}	C_{ds}	R_i
0.0128	1.5 ps	0.29 pF	0.036 pF	0.031 pF	4.9 Ω
v_{fcg}	f_{c1}	f_{c2}	c_v	f_{c3}	f_{c4}
4.7612	0.3780	2.4	0.0142	0.6320	0.3659
V_{dso}	V_{gso}	C_{pgs}	C_{pgd}	C_{pds}	R_{ds}
4.0 V	-4.03 V	0.003 pF	0.004 pF	0.005 pF	337.5 Ω
R_g	R_s	R_d	L_g	L_s	L_d
6.68 Ω	3.6 Ω	4 Ω	39 pH	0 pH	80.4 pH

the drain-bias voltage where the coefficients A_i $(i = 0, 1, 2, 3)$ are extracted. The gate-to-source capacitance is described by

$$C_{\rm gs} = C_{\rm gso}\left(\frac{1 + f_{c1}\tanh\left(f_{c2}(V_{\rm in} + v_{fcg})\right)}{1 + f_{c1}\tanh\left(f_{c2}(V_{\rm gso} + v_{fcg})\right)}\right) \cdot \left(\frac{1 + c_v V_{\rm out}}{1 + c_v V_{\rm dso}}\right) \quad (18)$$

and the gate-to-drain capacitance is

$$C_{\rm gd} = C_{\rm gdo}\frac{1 - f_{c3}\tanh(f_{c4}V_{\rm out})}{1 - f_{c3}\tanh(f_{c4}V_{\rm dso})} \quad (19)$$

where $V_{\rm gso}$ and $V_{\rm dso}$ are the bias voltages used for the $C_{\rm gso}$ and $C_{\rm gdo}$ extraction, and f_{c1}, f_{c2}, f_{c3}, f_{c4}, c_v, and v_{fcg} are fitting parameters. Table I lists the extracted parameters for the 0.25 × 250 μm^2 AlGaN/GaN HEMT we studied, obtained by fitting the analytic equations (16), (18), and (19) to the measured dc I–V curves and the bias-dependent small-signal scattering parameter data by means of a nonlinear curve fit using MATLAB. These extracted parameters were incorporated into a user-defined model in Agilent EEsof ADS.[1]

Equations (2) and (16) have a similar mathematical form, where g_{m1} and g_{m2} in (2) correspond to the ac components of the A_1 and A_2 terms in (16) if the dependence of $I_{\rm ds}$ on $V_{\rm out}$ in (16) can be neglected. Note that while (1) and (2) are employed to capture the basic concept of transistor nonlinearities, the nonlinear expressions (16) and (18) for $I_{\rm ds}$ and $C_{\rm gs}$ have cubic and hyperbolic tangent terms, representing higher order nonlinearities than those in (1) and (2) for more accurate modeling. Note that in (18) that $C_{\rm gs}$ is a function of not only $V_{\rm in}$, but also $V_{\rm out}$. Furthermore, in comparison to Fig. 1 with the noise source $(n(t))$ only at the input, the equivalent circuit in Fig. 2 includes additional noise sources, i.e., the intrinsic input and output noise sources (i_g, i_d) and the extrinsic device parasitics (R_g, R_s, R_d), which generate the extrinsic thermal noise.

Three independent noise mechanisms have been identified that can be represented as equivalent gate and drain noise current sources, as shown in Fig. 2 [18]. The velocity fluctuation ($i_{g,v}$ and $i_{d,v}$) is due to the electron scatter in the channel. The $1/f$ noise ($i_{g,1/f}$ and $i_{d,1/f}$) results from the trapping and reemitting of electrons due to surface or interface states.

[1]Agilent Advanced Design System, Circuit Simulation, Agilent EEsof, Agilent EEsof High-Frequency Design Solutions, Palo Alto, CA, 2004.

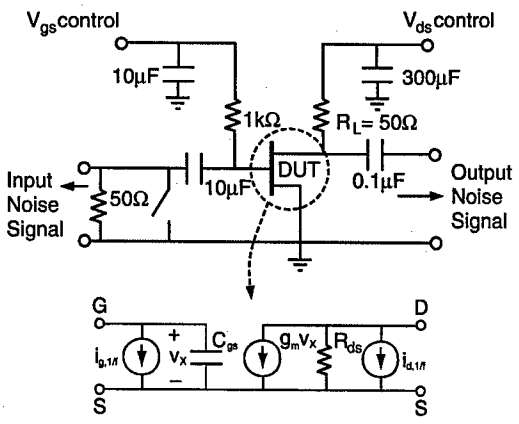

Fig. 3. Low-frequency $1/f$ noise measurement setup and a simplified equivalent circuit for the DUT (AlGaN/GaN HEMT) with the $1/f$ noise sources ($i_{g,1/f}$ and $i_{d,1/f}$) at the input and output.

The gate leakage shot noise ($i_{g,\rm shot}$ and $i_{d,\rm shot}$) is associated with the randomness of the electron injection into the channel over the gate Schottky barrier. The gate and drain noise variance ($\langle|i_g|^2\rangle$ and $\langle|i_d|^2\rangle$) and their correlation in terms of $C\left(=\langle i_g i_d^*\rangle / \sqrt{\langle|i_g|^2\rangle\langle|i_d|^2\rangle}\right)$ are incorporated into the noise model, and the values for each noise mechanism (velocity fluctuation, gate leakage, $1/f$ noise) were obtained by using the measured noise-figure parameters and a subsequent deembedding routine, a step taken in a prior study [18]. The extrinsic thermal noise (due to R_g, R_s, and R_d) was modeled using Nyquist's theorem [$\langle|i|^2\rangle = 4kT_0BR$, where k is the Boltzmann's constant, T_0 is the room temperature (290 K), and B is the noise bandwidth (1 Hz)] [21]. The model of Fig. 2 with linear elements correctly predicts the measured frequency-dependent microwave noise from 0.8 to 5.8 GHz [18].

Under large-signal conditions, the most critical sideband noise is that within a few megahertz of the fundamental carrier. The primary source of this noise is the up-conversion of $1/f$ noise, which is the single dominant noise mechanism in an FET at baseband, being larger than velocity fluctuation noise, gate leakage current noise, and thermal noise from the parasitics. Therefore, accurate determination of the intrinsic $1/f$ noise sources below a few megahertz is necessary for large-signal noise modeling.

In order to determine both $i_{g,1/f}$ and $i_{d,1/f}$ and their correlation in the equivalent circuit for the AlGaN/GaN HEMT device-under-test (DUT), we built a low-frequency $1/f$ noise measurement setup, and its schematic is displayed in Fig. 3. In the measurement frequency range (200 Hz–1 MHz), most parasitics in Fig. 2 and their thermal noise contribution can be ignored, and the simplified FET model in Fig. 3 is a reasonable approximation. The noise voltages across the 50-Ω gate termination and the ac drain load, i.e., $R_{\rm ds}//R_L$, are the input and output noise signals, and their noise power per unit bandwidth was measured using a low-frequency spectrum analyzer (HP3585A with a 1-MΩ input impedance, which displays noise power as dBm/Hz). This data was converted to current variance $\langle|i(\omega)|^2\rangle(\rm A^2/Hz)$, a suitable representation for the intrinsic noise sources in the equivalent circuit.

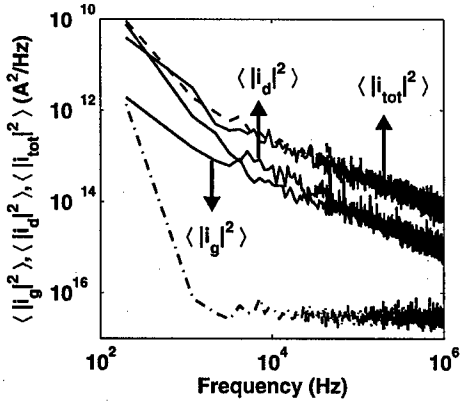

Fig. 4. Measured noise variances ($\langle|i_g|^2\rangle$, $\langle|i_d|^2\rangle$, and $\langle|i_{\rm tot}|^2\rangle$) for the AlGaN/GaN HEMT from 200 Hz to 1 MHz with $V_{\rm ds} = 3.1$ V and $V_{\rm gs} = -3.6$ V. The dashed line is the estimated $\langle|i_{\rm tot}|^2\rangle$ using the measured $\langle|i_g|^2\rangle$ and $\langle|i_d|^2\rangle$, applied to (20), neglecting the correlation term $\Re\left\{\left\langle i_{g,1/f} i^*_{d,1/f}\right\rangle\right\}$. The dashed–dotted line is the measurement system noise floor.

First, in order to obtain the drain noise current variance ($\langle|i_{d,1/f}|^2\rangle$), the shunt noise current at the input is shorted (with the switch closed in Fig. 3), allowing measurement of the drain noise current variance only, without the influence of the gate noise current. Second, for determination of $\left\langle|i_{g,1/f}|^2\right\rangle$, the gate circuit is terminated with 50 Ω (with the switch open in Fig. 3). By using the 50-Ω termination, a relatively low impedance ($|1/j\omega C_{\rm gs}| \gg 50\ \Omega$), most of $i_{g,1/f}$ will flow in the 50-Ω load, and $\left\langle|i_{g,1/f}|^2\right\rangle$ can be measured. Third, with the 50-Ω gate termination (and the switch open), $v_x \simeq 50 i_{g,1/f}$. Thus, the additional current ($50 g_m i_{g,1/f}$), along with the drain noise current source $i_{d,1/f}$, can be measured as a total output noise current variance $\left\langle|i_{\rm tot}|^2\right\rangle$ given by

$$\begin{aligned}\left\langle|i_{\rm tot}|^2\right\rangle &= \left\langle|50 g_m i_{g,1/f} + i_{d,1/f}|^2\right\rangle \\ &= (50 g_m)^2 \left\langle|i_{g,1/f}|^2\right\rangle + \left\langle|i_{d,1/f}|^2\right\rangle \\ &\quad + 100 g_m \Re\left\{\left\langle i_{g,1/f} i^*_{d,1/f}\right\rangle\right\} \end{aligned} \tag{20}$$

where $\left\langle|i_{g,1/f}|^2\right\rangle$, $\left\langle|i_{d,1/f}|^2\right\rangle$, and $\left\langle|i_{\rm tot}|^2\right\rangle$ are the measured quantities, g_m is the small-signal transconductance at a given bias point, and $\Re\{\ \}$ is the real part. We used the g_m determined from scattering-parameter data at microwave frequencies in (20), assuming that it is invariant between the low-frequency and microwave regime.

Fig. 4 shows the measured low-frequency $\left\langle|i_g|^2\right\rangle$, $\left\langle|i_d|^2\right\rangle$, and $\left\langle|i_{\rm tot}|^2\right\rangle$ for the $0.25 \times 250\ \mu{\rm m}^2$ AlGaN/GaN HEMT. The resolution bandwidth was set at 100 Hz for the measurement. The observed noise is of a $1/f^\alpha$ type, where $\alpha = 0.8$–1.0 under various bias conditions over the entire measurement frequency range (200 Hz–1 MHz). As shown in Fig. 4, our measurement results for $\left\langle|i_g|^2\right\rangle$, $\left\langle|i_d|^2\right\rangle$, and $\left\langle|i_{\rm tot}|^2\right\rangle$, applied to (20), indicates that the correlation term $\Re\{\langle i_{g,1/f} i^*_{d,1/f}\rangle\}$ is negligible.

For the imaginary part of $\langle i_{g,1/f} i^*_{d,1/f}\rangle$, one may anticipate correlation between $i_{g,1/f}$ and $i_{d,1/f}$ by capacitive coupling between the gate and channel [18], i.e., that i_d induces the gate noise voltage v_g through transconductance, resulting in $v_g = i_d/g_m$ (if perfect correlation can be assumed). Then, $i_g = j\omega C_{\rm gs} i_d/g_m$. This correlation assumption gives

$$\left\langle|i_g|^2\right\rangle = \frac{\omega^2 C^2_{\rm gs}\left\langle|i_d|^2\right\rangle}{g^2_m}. \tag{21}$$

We have demonstrated experimentally that, in the case of velocity fluctuation, $\left\langle|i_{d,v}|^2\right\rangle$ is independent of frequency, i.e., it is white noise, and that $\left\langle|i_{g,v}|^2\right\rangle \propto \omega^2$ at microwave frequencies [18]. The bandwidth of the white noise $\left\langle|i_{d,v}|^2\right\rangle$ is proportional to the inverse of the scattering time (typically a fraction of a picosecond). The measured $\left\langle|i_{g,1/f}|^2\right\rangle$ in Fig. 4 ($\propto \omega^{-1}$) is not consistent with the contribution of drain-induced gate noise $\omega^2 C^2_{\rm gs}\left\langle|i_{d,1/f}|^2\right\rangle/g^2_m$ ($\propto \omega$) predicted by (21). This indicates that $i_{g,1/f}$ and $i_{d,1/f}$ originate mostly from independent (thus, uncorrelated) sources, and that the impact of any correlation between $i_{g,1/f}$ and $i_{d,1/f}$ is not significant. A similar result (no measurable correlation between $i_{g,1/f}$ and $i_{d,1/f}$) was found for an InP HEMT [22]. Therefore, in relation to the trapping effects on $1/f$ noise in AlGaN/GaN HEMTs, our measurement study suggests that the traps responsible for $i_{g,1/f}$ are distinct from the traps responsible for $i_{d,1/f}$. Note that this is in contrast to velocity fluctuation noise, where our previous study highlighted the importance of correlation [18]. It is likely that $i_{g,1/f}$ results from traps on the surface, in particular, the ungated region between the gate and source, and that $i_{d,1/f}$ primarily results from traps located near the channel (e.g., the AlGaN/GaN interface). Prior studies have shown that passivation with an Si_3N_4 layer improves the large-signal microwave performance [23] and results in lower $1/f$ noise [24], presumably by suppressing the surface states.

Note that stationarity is assumed for the intrinsic $1/f$ noise sources that are incorporated into the large-signal equivalent-circuit model. This assumption is valid as long as the bias level is well controlled, i.e., fixed in the amplifier configuration, since the $1/f$ noise current variance depends only on the dc bias. In the oscillator circuit, however, the bias level is unknown and may vary under strongly nonlinear conditions, and the assumption of stationarity has been revisited to model the intrinsic $1/f$ noise sources under such conditions [25], [26].

The noise variance for the velocity fluctuation and gate leakage shot noise, obtained under small-signal and, thus, stationary conditions, are used in the large-signal model without modification. The velocity fluctuation and gate leakage shot noise are, therefore, assumed to be band-limited, at least in terms of the model domain. Although the contribution of velocity fluctuation and gate leakage shot noise to the near-carrier sideband noise is negligible under large-signal operation, they provide an ultimate limitation on the microwave noise performance in the small-signal limit.

IV. Amplitude and Phase Noise

Fig. 5 shows the measurement setup, which discriminates between amplitude and phase noise by adjusting the phase difference between the local oscillator (LO) and RF signals. This measurement procedure employs the DUT as an amplifier rather than as an oscillator [1]. By allowing control of the input power (thus, the output power), operation frequency, and bias level, the

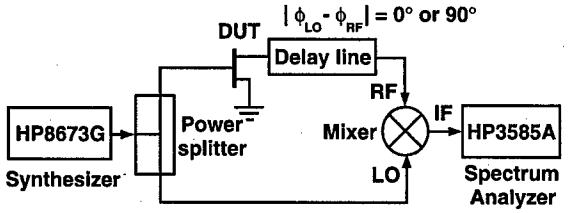

Fig. 5. Amplitude and phase-noise measurement setup with a line stretcher for electrical delay. A 2-GHz signal from a low-noise source is the input to the DUT, an AlGaN/GaN HEMT. All three ports of the power splitter and mixer are matched to 50 Ω.

amplifier configuration for the DUT allows a more complete investigation of the transistor nonlinearities. A 2-GHz signal from a synthesizer (HP8673G) is the input to the DUT, a 0.25-mm periphery AlGaN/GaN HEMT. The output signal from the DUT (RF) is mixed with the excitation (LO), and the down-converted spectrum (IF) is measured by a low-frequency spectrum analyzer (HP3585A, with a 50-Ω input impedance). At the mixer, the product of the LO and RF signals can be written as

$$i_{\rm IF}(t) = \Big(\big(I_0 + n_I(t)\big)\cos(\omega_0 t + \phi) - n_Q(t)\sin(\omega_0 t + \phi)\Big) \cdot I_{\rm LO}\cos(\omega_0 t) \quad (22)$$

where the LO signal is expressed as $I_{\rm LO}\cos(\omega_0 t)$, $i_{\rm RF}$ is a phase-shifted version of $I_0\cos(\omega_0 t) + n_0(t)$ with $n_0(t)$ given in (13), and ϕ is the phase shift between the RF and LO signals that is achieved by a line stretcher. The spectrum analyzer (HP3585A) measures the low-pass filtered (frequencies less than 40 MHz) form of (22), resulting in

$$i_{\rm IF}^{\rm LP}(t) = \frac{I_{\rm LO}(I_0 + n_I(t))\cos\phi}{2} - \frac{I_{\rm LO} n_Q(t)\sin\phi}{2}. \quad (23)$$

Equation (23) indicates that the dc voltage at the input of the spectrum analyzer (monitored by an HP3478A multimeter) is a maximum when the RF and LO signals are in-phase ($\phi = 0°$) and only $n_I(t)$ is measured, and that dc voltage is zero when they are in quadrature ($\phi = 90°$) and only $n_Q(t)$ is measured. The in-phase and quadrature (I/Q) power spectral densities can thus be obtained.

Fig. 6 shows the measured and simulated results for amplitude and phase noise (dBm/Hz) for the 0.25×250 μm^2 AlGaN/GaN HEMT as a function of the offset frequency from the carrier. Fig. 6 also shows the measured system noise floor (dotted line), summing noise contributions from every component used, except the DUT (the DUT was replaced with a through connection). The multiple spikes at lower frequencies result from the ac power supply (60 Hz) of the synthesizer. As shown in Fig. 6, the measured (solid line) amplitude and phase noise with $V_{\rm ds} = 4$ V and $I_{\rm ds} = 20$ mA both exhibit a $1/f^{\alpha}$-type spectrum, where $\alpha \simeq 1$ for offset frequencies from 50 Hz to 5 kHz.

To validate the model, the large-signal equivalent circuit of Fig. 2 was incorporated into a harmonic-balance simulator, which calculates the in-phase (n_I) and quadrature-phase noise (n_Q). Fig. 7 displays the simulation bench (Agilent EEsof ADS was used), where a 2.4-dBm 2-GHz signal (the same condition as in the measurement) was provided as an input to

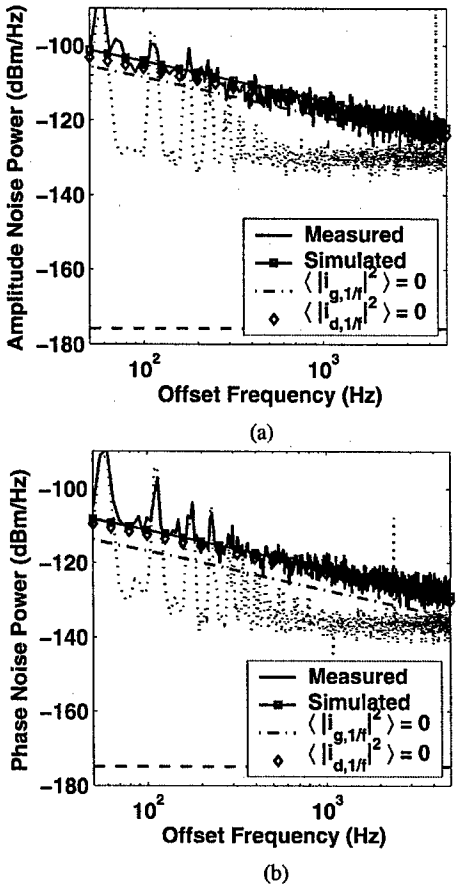

Fig. 6. Measured and simulated: (a) amplitude and (b) phase noise for a 0.25-mm periphery AlGaN/GaN HEMT with $V_{\rm ds} = 4$ V and $I_{\rm ds} = 20$ mA ($V_{\rm gs} = -4.2$ V). The input power (to the DUT) is 2.4 dBm at 2 GHz, and the sideband noise at the output load (50 Ω) is measured and simulated in terms of power per normalized bandwidth (dBm/Hz). The long dashed lines are the simulated case with $\langle |i_{g,1/f}|^2 \rangle = \langle |i_{d,1/f}|^2 \rangle = 0$. The dotted lines are the measured system noise floor.

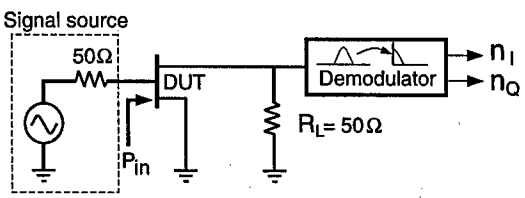

Fig. 7. Amplitude and phase-noise simulation bench. The DUT, a large-signal device model for a 0.25×250 μm^2 AlGaN/GaN HEMT, as shown in Fig. 2, is terminated with 50 Ω at the input and output, the same termination impedance as provided in the actual measurement.

the DUT, and the I/Q demodulator at the 50-Ω load produces two baseband output signals n_I and n_Q. The simulated results in Fig. 6 (square-solid line) show excellent agreement with the measured data. Setting both $i_{g,1/f}$ and $i_{d,1/f}$ in the model to zero produces frequency-independent velocity fluctuation noise and shot noise shown as the dashed line in Fig. 6. Under large-signal conditions, the velocity fluctuation noise is negligible at near-carrier sideband frequencies. It is also shown in Fig. 6 that $i_{g,1/f}$ is a more important noise contributor than $i_{d,1/f}$ because turning off $i_{g,1/f}$ only in the model results in a greater reduction in both the amplitude and phase noise

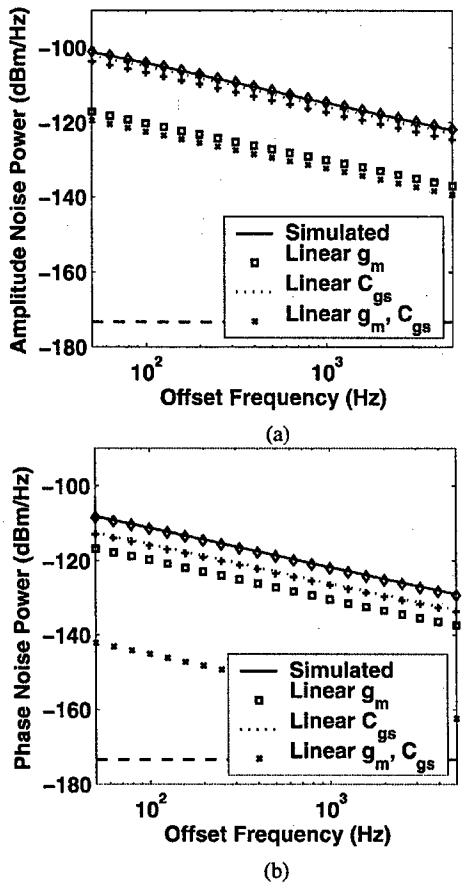

Fig. 8. Measured and simulated: (a) amplitude and (b) phase noise. The input power (to the DUT) is 2.4 dBm at 2 GHz. The squares and dotted lines are the cases with linear g_m and linear C_{gs}, respectively. The + symbols [note that they nearly overlap with dotted lines in (b)] are the case with 10% of the estimated input parasitic resistance R_g. The frequency-independent long dashed line is the case for a linear device.

(dashed–dotted lines) than turning off $i_{d,1/f}$ only (diamonds) in the simulation. However, it appears that the contribution of $i_{d,1/f}$ is appreciable. This output noise source appears as noise sidebands, due to mixing associated with either the drain–source nonlinearity or via gate–drain linear feedback and mixing from the gate–source nonlinear elements (it appears that the gate–drain nonlinearities have little impact).

After having established an accurate nonlinear equivalent-circuit model, it becomes possible to evaluate the impact that each circuit element has on the up-conversion. Consider the impact of the nonlinearities in (16) and (18) associated with dependencies on V_{in} and V_{out}. Fig. 8 shows the simulated amplitude and phase noise with the V_{in} dependency removed from $g_m(=((\partial I_{\text{ds}}(V_{\text{in}}, V_{\text{out}}))/\partial V_{\text{in}}))$, making it approximately linear, and a linear C_{gs}. The value C_{gs} is set equal to C_{gso} by setting c_v and f_{c1} equal to zero in (18), making it linear. For g_m, expressed by (16), A_2 and A_3 were set to zero, resulting in g_m becoming independent of V_{in}. The dependency on V_{out}, which relates to the description of the nonlinear output conductance $(=((\partial I_{\text{ds}}(V_{\text{in}}, V_{\text{out}}))/\partial V_{\text{out}}))$, is relatively weak. As a consequence of these steps, Fig. 8(a) shows that the amplitude noise is appreciably reduced with an approximately linear g_m, but not greatly with a linear C_{gs}. On the other hand, Fig. 8(b) shows that the phase noise can be significantly reduced by linearizing both g_m and C_{gs}, i.e., both nonlinearities are important contributors to the phase noise. The diamonds in Fig. 8, which virtually overlap with the solid lines, are the case where C_{gd} was linearized by setting f_{c3} equal to zero in (19). This simulation study indicates that linearization of C_{gd} has little effect on the amplitude and phase noise. With the removal of the V_{in} dependence from both g_m and C_{gs}, the noise in Fig. 8 is substantially reduced (the x marks in Fig. 8). Remaining are the relatively small contributions due to the V_{out} dependency and the drain–source and grate–drain nonlinearities. Finally, the frequency-independent long dashed lines in Fig. 8 are the case for a perfectly linear device, where no $1/f$ noise up-conversion occurs.

Consider again the simplified analytical model of Section II, which yielded the I/Q noise expressions of (14) and (15), which assumed only an input equivalent noise source. The minimal impact of the linear C_{gs} on the amplitude noise in Fig. 8(a) suggests that $RC_2 \ll 1$ in (14) and that, indeed, the first term, which is associated only with the nonlinear transconductance, is dominant. This is consistent with the assumption made in earlier research [13]. The significant impact of linearizing both g_m and C_{gs} in the phase noise of Fig. 8(b) suggests that both terms in (15) are significant. Note that this observation is in contradiction with previous assumptions that phase noise is due to the nonlinear capacitance, and the contribution from the nonlinear transconductance can be neglected [13].

To evaluate the impact of reducing the gate parasitic resistance R_g, the + symbols in Fig. 8 show the simulated amplitude and phase-noise performances with 10% of the extracted gate parasitic resistance. As indicated in this figure [and in (14) and (15)], the near-carrier sideband noise, in particular, the phase noise, can be reduced by reducing the gate metal resistance. It was found in our simulation that lowering the channel resistance R_i has little effect on the sideband noise (although from Table I, both resistances have similar size). This is a consequence of V_{in}, the voltage across C_{gs} and R_i, modulating C_{gs} [see (18)] in the particular nonlinear model we used. The point to note is the impact of the gate resistance on the noise properties, established through both the more general nonlinear model of Fig. 2 and the simple model of Fig. 1. While the contribution of thermal noise introduced by the parasitics to the near-carrier sideband noise is negligible, the input parasitic resistance has a significant impact on both the amplitude noise and phase noise through the device nonlinearities.

V. Conclusion

The emphasis of this study was to establish the precise relation between the intrinsic noise sources and the near-carrier sideband noise in terms of the transistor nonlinearities. A simplified analytical model for the in-phase amplitude noise and quadrature phase noise provides the qualitative picture, which has been supported with a more general nonlinear model, that the amplitude noise is dominated by the nonlinear transconductance and the phase noise has important contribution from the gate capacitance nonlinearity, as well as the nonlinear transconductance. As the gate parasitic resistance provides the

vehicle that produces that phase noise, one can expect that reducing the gate contact resistance will have significant impact on oscillator noise performance. Both the input and output noise sources appear significant and should be incorporated into nonlinear device noise models. Although the nonlinear model was validated only for an AlGaN/GaN HEMT, it appears that this view should be applicable to all FETs. The example large-signal model used works effectively, and allowed the impact of physical noise sources and nonlinearities to be evaluated. It should be able to accurately model FETs during the design of, for example, oscillators.

ACKNOWLEDGMENT

The authors would like to thank Prof. L. F. Eastman, Cornell University, Ithaca, NY, and Dr. V. Tilak, now with General Electric (GE), Niskayuna, NY, for device fabrication, and Dr. W. R. Curtice, W. R. Curtice Consulting, Washington Crossing, PA, for donation of the CFET model package.

REFERENCES

[1] P. A. Dallas and J. K. A. Everard, "Characterization of flicker noise in GaAs MESFET's for oscillator applications," *IEEE Trans. Microw. Theory Tech.*, vol. 48, no. 2, pp. 245–257, Feb. 2000.

[2] M. N. Tutt, D. Pavlidis, A. Khatibzadeh, and B. Bayraktaroglu, "The role of baseband noise and its upconversion in HBT oscillator phase noise," *IEEE Trans. Microw. Theory Tech.*, vol. 43, no. 7, pp. 1461–1471, Jul. 1995.

[3] D. B. Leeson, "A simple model of feedback oscillator noise spectrum," *Proc. IEEE*, vol. 54, no. 2, pp. 329–330, Feb. 1966.

[4] R. A. Pucel and J. Curtis, "Near-carrier noise in FET oscillators," in *IEEE MTT-S Int. Microwave Symp. Dig.*, 1983, pp. 284–284.

[5] J. Verdier, O. Llopis, R. Plana, and J. Graffeuil, "Analysis of noise up-conversion in microwave field-effect transistor oscillators," *IEEE Trans. Microw. Theory Tech.*, vol. 44, no. 8, pp. 1478–1483, Aug. 1996.

[6] T. H. Lee and A. Hajimiri, "Oscillator phase noise: A tutorial," *IEEE J. Solid-State Circuits*, vol. 35, no. 3, pp. 326–336, Mar. 2000.

[7] A. Laloue, A. Lyoubi, M. Camiade, J. C. Nallatamby, M. Valenza, M. Prigent, and J. Obregon, "A measurement based distributed low frequency noise HEMT model: Application to design of millimeter wave automotive radar chip sets," in *IEEE MTT-S Int. Microwave Symp. Dig.*, Phoenix, AZ, May 2001, pp. 423–426.

[8] O. Llopis, J. B. Juraver, B. Tamen, F. Danneville, M. Chaubet, A. Cappy, and J. Graffeuil, "Nonlinear noise modeling of a PHEMT device through residual phase noise and low frequency noise measurements," in *IEEE MTT-S Int. Microwave Symp. Dig.*, Phoenix, AZ, May 2001, pp. 831–834.

[9] G. Cibiel, M. Regis, O. Llopis, A. Rennane, L. Bary, R. Plana, Y. Kersale, and V. Giordano, "Optimization of an unltra low-phase noise sapphire–SiGe HBT oscillator using nonlinear CAD," *IEEE Trans. Ultrason., Ferroelect., Freq. Control*, vol. 51, no. 1, pp. 33–41, Jan. 2004.

[10] D. R. Pehlke, A. Sailer, W. J. Ho, J. A. Higgins, H. Smith, J. Hebert, and M. Vineyard, "A predictive model describing the upconversion of $1/f$ noise into AM sideband noise in HBT's," in *Device Research Conf. Dig.*, 1995, pp. 94–95.

[11] S. Lee, K. J. Webb, and L. F. Eastman, "The influence of transistor nonlinearities on intrinsic noise," in *IEEE MTT-S Int. Microwave Symp. Dig.*, Fort Worth, TX, Jun. 2004, pp. 1867–1870.

[12] B. T. Debney and J. S. Joshi, "A theory of noise in GaAs FET microwave oscillators and its experimental verification," *IEEE Trans. Electron Devices*, vol. 30, no. 7, pp. 769–772, Jul. 1983.

[13] H. J. Siweris and B. Schiek, "Analysis of noise upconversion in microwave FET oscillators," *IEEE Trans. Microw. Theory Tech.*, vol. MTT-33, no. 3, pp. 233–242, Mar. 1985.

[14] L. F. Eastman, V. Tilak, J. Smart, B. M. Green, E. M. Chumbes, R. Dimitrov, H. Kim, O. S. Ambacher, N. Weimann, T. Prunty, M. Murphy, W. J. Schaff, and J. R. Shealy, "Undoped AlGaN/GaN HEMT's for microwave power amplification," *IEEE Trans. Electron Devices*, vol. 48, no. 3, pp. 479–485, Mar. 2001.

[15] W. B. Davenport and W. L. Root, *An Introduction to the Theory of Random Signals and Noise*. New York: McGraw-Hill, 1958.

[16] S. Haykin, *Communications Systems*, 3rd ed. New York: Wiley, 1994.

[17] P. Penfield, "Circuit theory of periodically driven nonlinear systems," *Proc. IEEE*, vol. 54, no. 2, pp. 266–280, Feb. 1966.

[18] S. Lee, K. J. Webb, V. Tilak, and L. F. Eastman, "Intrinsic noise equivalent circuit parameters for AlGaN/GaN HEMTs," *IEEE Trans. Microw. Theory Tech.*, vol. 51, no. 5, pp. 1567–1577, May 2003.

[19] W. R. Curtice and M. Ettenberg, "A nonlinear GaAs FET model for use in the design of output circuits for power amplifiers," *IEEE Trans. Microw. Theory Tech.*, vol. 33, no. 12, pp. 1383–1394, Dec. 1985.

[20] J. W. Lee and K. J. Webb, "A temperature-dependent nonlinear analytic model for AlGaN–GaN HEMTs on SiC," *IEEE Trans. Microw. Theory Tech.*, vol. 52, no. 1, pp. 2–9, Jan. 2004.

[21] H. Nyquist, "Thermal agitation of electric charge in conductors," *Phys. Rev.*, vol. 32, pp. 110–113, Jul. 1928.

[22] H. C. Duran, L. Ren, M. Beck, M. A. Py, M. Ilegems, and W. Bachtold, "Low-frequency noise properties of selectively dry etched InP HEMT's," *IEEE Trans. Electron Devices*, vol. 45, no. 6, pp. 1219–1225, Jun. 1998.

[23] B. M. Green, K. K. Chu, E. M. Chumbes, J. A. Smart, J. R. Shealy, and L. F. Eastman, "The effect of surface passivation on the microwave characteristics of undoped AlGaN/GaN HEMT's," *IEEE Electron Device Lett.*, vol. 21, no. 6, pp. 268–270, Jun. 2000.

[24] A. V. Vertiatchikh and L. F. Eastman, "Effect of the surface and barrier defects on the AlGaN/GaN HEMT low-frequency noise performance," *IEEE Electron Device Lett.*, vol. 24, no. 9, pp. 535–537, Sep. 2003.

[25] J. E. Sanchez, G. Bosman, and M. E. Law, "Two-dimensional semiconductor device simulation of trap-assisted generation-recombination noise under periodic large-signal conditions and its use for developing cyclostationary circuit simulation models," *IEEE Trans. Electron Devices*, vol. 50, no. 5, pp. 1353–1362, May 2003.

[26] M. Margraf and G. Boeck, "Analysis and modeling of low-frequency noise in FET mixers," *IEEE Trans. Microw. Theory Tech.*, vol. 52, no. 7, pp. 1709–1717, Jul. 2004.

Sungjae Lee (S'98–M'04) received the B.S. degree in electrical engineering from Seoul National University, Seoul, Korea, in 1998, and the M.S. and Ph.D. degrees from Purdue University, West Lafayette, IN, in 2000 and 2004, respectively. His graduate research concerned broad-band power-amplifier design, and noise characterization and modeling of AlGaN/GaN HEMTs.

During Summer 2001, he was an Intern with Digital DNA Laboratories, Motorola Inc., Tempe, AZ. In 2004, he joined IBM Microelectronics, Essex Junction, VT.

Dr. Lee is a member of Eta Kappa Nu.

Kevin J. Webb (S'81–M'84–SM'98–F'05) received the B.Eng. and M.Eng. degrees from the Royal Melbourne Institute of Technology, Melbourne, Australia, in 1978 and 1983, respectively, the M.S.E.E. degree from the University of California at Santa Barbara, in 1981, and the Ph.D. degree from the University of Illinois at Urbana-Champaign, in 1984.

He is currently a Professor with the School of Electrical and Computer Engineering, Purdue University, West Lafayette, IN.

A correlated diffusion noise model for the field-effect transistor

Sungjae Lee and Kevin J. Webb[‡]

School of Electrical and Computer Engineering, Purdue University, West Lafayette, IN 47907

Abstract

A numerical approach to simulate the intrinsic noise sources within transistors is described, and the impact of spatial correlation between local fluctuations is investigated. Using a two-dimensional numerical device solver, spectral densities for the gate and drain noise current sources and their correlation are evaluated using a Green's function approach, an equivalent of Shockley's impedance field method. Case studies with an AlGaN/GaN high electron mobility transistor are supported by measurement data. While local velocity fluctuations are correlated, their impact on terminal noise is found identical to the one generated by assuming uncorrelated diffusion noise source. Therefore, using uncorrelated local fluctuation to calculate the intrinsic noise sources is found to be valid even for the sub-micron gate length FET studied.

Index Terms

Semiconductor device noise, numerical analysis, Green's function, diffusion processes, correlation, noise measurement.

[†]Submitted to IEEE Transactions on Electron Devices, 06/02/04

[‡]Electrical Engineering Building, 465 Northwestern Ave. West Lafayette, IN 47907

Email: webb@purdue.edu, Phone: 765 494-3373, Fax: 765 494-2706

I. Introduction

Transistor noise presents a critical limitation, dictating, for example, receiver sensitivity and transmitter sideband noise. Measurements with an equivalent circuit model allows establishing a link to physical aspects of the device through circuit elements. A more complete interrogation of the device noise can be established using numerical models for the noise sources. The impedance field method for numerical transistor noise modeling, first proposed by Shockley [1], involves the determination of the Green's function (or impedance field), i.e., the influence of a local fluctuation (in terms of current or voltage at one point in the channel) at the gate and drain terminals, in the case of the field-effect transistor (FET). This method has enabled the intrinsic noise sources (gate and drain noise sources and their correlation) to be determined [2], [3].

In the impedance field method, the channel is divided into many segments for numerical simulation. For long channel devices, the volume of each segment can be sufficiently large so that local velocity fluctuations can be assumed to be spatially uncorrelated between segments. This assumption of uncorrelated noise sources has been commonly used to simplify the problem and to calculate the intrinsic noise sources [1], [2], [4]. However, as the device and segment size shrinks, local noise sources (due to velocity fluctuation) between segments can be correlated because a significant number of electrons can travel between nearby segments without their velocity being randomized significantly [5].

The spatial correlation between local velocity fluctuations has been studied numerically. The two-point cross-correlation function of velocities at different spatial positions can be related to the probability that electrons travel between points without their velocity being randomized by scattering events [6]. With a Monte-Carlo simulation, the cross-correlation function of the velocity fluctuations in different segments inside a one-dimensional (1-D) GaAs structure was obtained by tracking the kinetics of individual electrons within the device [7], [8]. This demonstrated the practical importance of retaining correlations between the noise sources in neighboring segments.

In this paper, a two-dimensional (2-D) numerical approach is presented in order to investigate the effect of spatially correlated local noise sources on the gate and drain terminal noise in the FET geometry. While Monte-Carlo simulation can determine the numerical values of the spatially correlated local noise sources [7], several studies have found that the assumption of uncorrelated diffusion noise source is sufficient to determine gate and drain noise sources in the FET numerically even for the sub-micron gate length devices considered [9], [10]. The focus of our work is to investigate how spatial correlation between local fluctuations affects terminal noise, not to determine physical local noise sources that are correlated. Our proposed approach is in the framework of the drift-diffusion model that we find valid for noise modeling. Using this model, diffusion noise sources and Green's functions are determined. We assume that the independent (uncorrelated) local diffusion noise sources that are initially obtained from the drift-diffusion model are, in fact, comprised of contributions from correlated noise terms involving the nearby segments. Then, the coupling of the local noise sources (either correlated or uncorrelated) to the gate and drain terminal in the FET is simulated using the Green's function approach to study the merit of

assuming spatially correlated noise sources. We use the example of an aluminum gallium-nitride/gallium-nitride high electron mobility transistor (AlGaN/GaN HEMT) that was fabricated as part of a program to develop high power microwave sources and amplifiers [11]. The high mobility in the 2-D electron gas (2DEG) not only results in high operating frequencies, but also low microwave noise, making AlGaN/GaN HEMTs suitable for low noise receivers, hence the interest in their microwave noise properties [12].

We develop the correlated diffusion noise theory in Section II. The discrete implementation of the model, with a simple correlation assumption implemented, is described in Section III. Section IV applies this model to an AlGaN/GaN HEMT and compares the terminal noise predicted with that from measurements.

II. Theory

A. Velocity Fluctuation

The noise random processes $n_1(t)$ and $n_2(t)$, where the subscripts indicate vector component or position vectors, are considered as representing electron velocity, current, or voltage. We write the means as $\langle n_1(t)\rangle$ and $\langle n_2(t)\rangle$, where $\langle\rangle$ denotes the statistical average, the cross-correlation function as $\langle n_1(t)n_2(t+\tau)\rangle$, and the cross power spectral density as $\langle n_1 n_2^*\rangle$, where * denotes the complex conjugate.

In the case of the FET, the velocity fluctuation is primarily due to electron scatter from the lattice (phonons) and impurities in the channel. The random velocity deviation, $\mathbf{u}(\mathbf{r}_k,t)$ at position $\mathbf{r}_k$ and time t, generates the zero-mean noise current density $\mathbf{j}(\mathbf{r}_k,t)$ (A/cm^2) by

$$\begin{aligned}\mathbf{j}(\mathbf{r}_k,t) &= qn_k\mathbf{u}(\mathbf{r}_k,t)\\ &= \lim_{\Delta\nu_k\to 0}\sum_i \frac{1}{\Delta\nu_k} q\ \mathbf{u}_i(\mathbf{r}_k,t),\end{aligned} \tag{1}$$

where q is the absolute value of electron charge (-1.6×10^{-19} C), n_k (cm^{-3}) is the charge density at $\mathbf{r}_k$, and the subscript i denotes the i-th carrier within the volume $\Delta\nu_k$ that encloses $\mathbf{r}_k$. Using (1), the two-point ($\mathbf{r}_k$, $\mathbf{r}_l$) cross-correlation function of the noise current density is

$$\langle j_\alpha(\mathbf{r}_k,t)j_\beta(\mathbf{r}_l,t+\tau)\rangle = \lim_{\Delta\nu_{k,l}\to 0}\sum_i\sum_j q^2\frac{1}{\Delta\nu_k}\frac{1}{\Delta\nu_l}\langle u_{i\alpha}(\mathbf{r}_k,t)u_{j\beta}(\mathbf{r}_l,t+\tau)\rangle, \tag{2}$$

where the subscripts α and β indicate the projections of $\mathbf{j}$ along the directions α and β. Assuming no correlation between different electrons (and thus their velocities) [6], (2) becomes

$$\langle j_\alpha(\mathbf{r}_k,t)j_\beta(\mathbf{r}_l,t+\tau)\rangle = \lim_{\Delta\nu_{k,l}\to 0}\sum_i q^2\frac{1}{\Delta\nu_k}\frac{1}{\Delta\nu_l}\langle u_{i\alpha}(\mathbf{r}_k,t)u_{i\beta}(\mathbf{r}_l,t+\tau)\rangle, \tag{3}$$

which means that $\langle j_\alpha(\mathbf{r}_k,t)j_\beta(\mathbf{r}_l,t+\tau)\rangle$ is nonzero only if the electrons can travel from $\mathbf{r}_k$ to $\mathbf{r}_l$ after time τ has passed without their velocity being completely randomized.

We assume a zero mean wide-sense stationary random process $\mathbf{u}$ (and thus $\mathbf{j}$), so that $\langle u_{i\alpha}(\mathbf{r}_k,t)u_{i\beta}(\mathbf{r}_l,t+\tau)\rangle$ is independent of t and forms a Fourier transform pair with $\langle u_{i\alpha}(\mathbf{r}_k)u_{i\beta}^*(\mathbf{r}_l)\rangle$ [13]. Taking Fourier transforms of

both sides of (3) gives

$$\langle j_\alpha(\mathbf{r}_k) j^*_\beta(\mathbf{r}_l)\rangle = \lim_{\Delta\nu_{k,l}\to 0} \sum_i q^2 \frac{1}{\Delta\nu_k}\frac{1}{\Delta\nu_l}\langle u_{i\alpha}(\mathbf{r}_k) u^*_{i\beta}(\mathbf{r}_l)\rangle. \tag{4}$$

From (4), the noise diffusion coefficient $D_{\alpha\beta}$ can be defined as [14]

$$\begin{aligned} D_{\alpha\beta}(\mathbf{r}_k, \mathbf{r}_l, \omega) &= \frac{1}{2}\langle u_{i\alpha}(\mathbf{r}_k) u^*_{i\beta}(\mathbf{r}_l)\rangle \\ &= \frac{1}{2}\int_{-\infty}^{\infty} \langle u_{i\alpha}(\mathbf{r}_k, t) u_{i\beta}(\mathbf{r}_l, t+\tau)\rangle e^{-j\omega\tau}\, d\tau, \end{aligned} \tag{5}$$

where the subscript i is dropped from the noise diffusion coefficient since $D_{\alpha\beta}(\mathbf{r}_k, \mathbf{r}_l, \omega)$ is assumed to be identical for every electron within the volume $\Delta\nu_k$, observed at t. For $|\tau| \gg \tau_s$ in (5), where τ_s is the mean-free time (typically a fraction of ps) between collisions, the electron loses memory of its initial velocity after several collisions, i.e., electron velocity becomes randomized, and thus the cross-correlation function, $\langle u_\alpha(t) u_\beta(t+\tau)\rangle$, becomes negligible. The bandwidth of this random process is proportional to the inverse of the scattering time, τ_s. Therefore, for microwave frequencies where $\omega\tau \ll 1$ and $e^{-j\omega\tau} \simeq 1$,

$$D_{\alpha\beta}(\mathbf{r}_k, \mathbf{r}_l) \simeq \frac{1}{2}\int_{-\infty}^{\infty} \langle u_{i\alpha}(\mathbf{r}_k, t) u_{i\beta}(\mathbf{r}_l, t+\tau)\rangle\, d\tau, \tag{6}$$

which is frequency independent (i.e., white noise) in the microwave regime where we have performed numerical simulations. Note that the lower frequency (microwave) result for the noise diffusion coefficient in (6) can be demonstrated to be identical to the spreading diffusion coefficient ($D_{\alpha\beta} = \frac{1}{2}\langle \Delta r_\alpha(t) \Delta r_\beta(t)\rangle$, where $\Delta r = |\mathbf{r}_k - \mathbf{r}_l|$), defined first by Einstein for Brownian motion [15] and applied in drift-diffusion carrier transport models [14].

Applying (5) to (4) gives

$$\begin{aligned} \langle j_\alpha(\mathbf{r}_k) j^*_\beta(\mathbf{r}_l)\rangle &= \lim_{\Delta\nu_{k,l}\to 0} \sum_i 2q^2 \frac{1}{\Delta\nu_k}\frac{1}{\Delta\nu_l} D_{\alpha\beta}(\mathbf{r}_k, \mathbf{r}_l, \omega) \\ &= \lim_{\Delta\nu_l \to 0} 2q^2 n_k \frac{1}{\Delta\nu_l} D_{\alpha\beta}(\mathbf{r}_k, \mathbf{r}_l, \omega). \end{aligned} \tag{7}$$

Generalizing (7) for vector quantities ($\mathbf{u}$ and $\mathbf{j}$),

$$\langle \mathbf{j}(\mathbf{r}_k)\mathbf{j}^*(\mathbf{r}_l)\rangle = \lim_{\Delta\nu_l \to 0} 4q^2 n_k \frac{1}{\Delta\nu_l} \mathbf{D}(\mathbf{r}_k, \mathbf{r}_l, \omega), \tag{8}$$

where $\langle \mathbf{j}(\mathbf{r}_k)\mathbf{j}^*(\mathbf{r}_l)\rangle$ and $\mathbf{D}(\mathbf{r}_k, \mathbf{r}_l, \omega)$ are tensors. The factor of 4 (instead of 2) in (8) assumes that frequency encompasses only positive values, since the power spectral density for real random processes is even in frequency (i.e., the Fourier transform assigns half the power to negative frequencies and half to positive frequencies) [13]. The current density deviation correlation $\langle \mathbf{j}(\mathbf{r}_k)\mathbf{j}^*(\mathbf{r}_l)\rangle$ in (8) is proportional to the spatially correlated diffusion noise source. Note that $\langle \mathbf{j}(\mathbf{r}_k)\mathbf{j}^*(\mathbf{r}_l)\rangle$ will diminish with increasing distance due to scatter, and will become negligible if the two points $\mathbf{r}_k$ and $\mathbf{r}_l$ are separated by more than several mean-free paths [4], [7]. If $\mathbf{j}(\mathbf{r}_k)$ and $\mathbf{j}(\mathbf{r}_l)$ are spatially uncorrelated, i.e., $\langle \mathbf{j}(\mathbf{r}_k)\mathbf{j}^*(\mathbf{r}_l)\rangle = 0$ when $\mathbf{r}_k \neq \mathbf{r}_l$, (8) can be simplified to

$$\langle \mathbf{j}(\mathbf{r}_k)\mathbf{j}^*(\mathbf{r}_l)\rangle = 4q^2 n_k \mathbf{D}(\mathbf{r}_k, \mathbf{r}_l, \omega)\delta(\mathbf{r}_k - \mathbf{r}_l), \tag{9}$$

where δ is the Dirac delta function.

B. Non-Equilibrium Noise

The current density correlation of (9) applied in 1-D results in the uncorrelated current spectral density

$$\langle |j(\mathbf{r})|^2 \rangle = 4q^2 n(\mathbf{r}) D(\mathbf{r}) \delta(\mathbf{r}). \tag{10}$$

The Einstein relation under thermal equilibrium gives $\frac{kT}{q} = \frac{D_0}{\mu_0}$, where k is Boltzmann's constant, T is the temperature, μ_0 is the low-field mobility, and D_0 is the spreading diffusion coefficient under equilibrium conditions. Therefore, at equilibrium, with use of the Einstein relation and $\sigma = q\mu n$, with σ being the conductivity, (10) becomes

$$\langle |j(\mathbf{r})|^2 \rangle = 4kT(\mathbf{r}) \sigma(\mathbf{r}) \delta(\mathbf{r}), \tag{11}$$

where $\sigma = \sigma_0$ is the low-field conductivity. The noise spectral density in (11) is consistent with the thermal noise source for a resistor developed by Nyquist [16], where $T = T_0$, the ambient temperature for the resistor, and σ_0 is the measured (DC) conductivity.

Consider now the non-equilibrium situation where all electrons are not at the lattice temperature and where there is a field-dependent mobility $\mu(E)$. Equation (11) can now be interpreted in terms of the differential conductance $\sigma(E)$, which is equivalent to applying the Einstein relation with the interpretation that D now represents the small signal noise diffusion process [4]. This view is consistent with the general velocity correlation interpretation of the diffusion coefficient in (5). In applying (11) to non-equilibrium processes, the temperature can be adjusted to produce the equivalent noise source (thus T becomes T_n, the noise temperature), or the differential noise conductance can be used with $T = T_0$, the ambient (lattice) temperature. Both approaches are common in noise equivalent circuit analysis [17], [18]. We take the latter approach in a drift-diffusion numerical implementation of noise sources.

C. Green's Function

The noise analysis presented in this paper is based on a Green's function approach, where, for the discretized linear device, Green's functions are obtained by solving Poisson's equation and the current continuity equations using a 2-D numerical device solver [19], [20]. Mathematically, Poisson's and the continuity equations are coupled since both equations include the charge density. The linearized equations about the steady-state solutions (potential, electron and hole densities) are

$$\mathcal{L}v(\mathbf{r}) = s(\mathbf{r}), \tag{12}$$

where $\mathcal{L}$ is the linearized differential operator for the coupled Poisson's and continuity equations and $v(\mathbf{r})$ is the perturbed potential due to the small signal stochastic source term $s(\mathbf{r})$. The Green's function for (12) satisfies

$$\mathcal{L}G(\mathbf{r}, \mathbf{r}_k) = \delta(\mathbf{r} - \mathbf{r}_k), \tag{13}$$

where $G(\mathbf{r}, \mathbf{r}_k)$ is the solution (response) at $\mathbf{r}$ to the spatially impulsive unit source $\delta(\mathbf{r} - \mathbf{r}_k)$. The solution of (12) is therefore

$$v(\mathbf{r}) = \int G(\mathbf{r}, \mathbf{r}_k) s(\mathbf{r}_k) \, d\nu_k. \tag{14}$$

We assume that the source term, s, results only from the noise current density due to the velocity fluctuation of the electrons in the channel. Thus, if there is no noise current density, no charge fluctuation occurs (by the continuity equation), which translates to zero perturbation at the observation point (by Poisson's equation). We do not consider other intrinsic noise mechanisms, for example, the gate leakage current shot noise and the trap-related $1/f$ noise. Since the current density appears in the continuity equation in the form of its divergence, we write the source term s as

$$s = \nabla \cdot \mathbf{j}. \tag{15}$$

Applying (15) to (14), we obtain the perturbed potentials at the device terminals as

$$v_p = \int G(\mathbf{r}_p, \mathbf{r}_k) \nabla \cdot \mathbf{j}(\mathbf{r}_k)\, d\nu_k \tag{16}$$

$$v_q = \int G(\mathbf{r}_q, \mathbf{r}_l) \nabla \cdot \mathbf{j}(\mathbf{r}_l)\, d\nu_l, \tag{17}$$

where p and q (or their location vectors, $\mathbf{r}_p$ and $\mathbf{r}_q$) denote either the gate or drain terminals in the FET. We assume the source terminal is grounded.

Applying the vector identity ($\nabla \cdot (x\mathbf{A}) = \mathbf{A} \cdot \nabla x + x \nabla \cdot \mathbf{A}$) and the divergence theorem, we can rewrite (16) (and likewise (17)) as

$$v_p = \oint_S G(\mathbf{r}_p, \mathbf{r}_k) \mathbf{j}(\mathbf{r}_k) \cdot d\mathbf{s} - \int \nabla G(\mathbf{r}_p, \mathbf{r}_k) \cdot \mathbf{j}(\mathbf{r}_k)\, d\nu_k. \tag{18}$$

Assuming no surface noise sources, the surface integral in (18) vanishes, resulting in [3]

$$v_p = -\int \nabla G(\mathbf{r}_p, \mathbf{r}_k) \cdot \mathbf{j}(\mathbf{r}_k)\, d\nu_k \tag{19}$$

$$v_q = -\int \nabla G(\mathbf{r}_q, \mathbf{r}_l) \cdot \mathbf{j}(\mathbf{r}_l)\, d\nu_l. \tag{20}$$

The cross-correlation voltage spectral density of the terminal noise voltages is then

$$\langle v_p v_q^* \rangle = \int \int \nabla G(\mathbf{r}_p, \mathbf{r}_k) \cdot \langle \mathbf{j}(\mathbf{r}_k) \mathbf{j}^*(\mathbf{r}_l) \rangle \cdot \nabla G^*(\mathbf{r}_q, \mathbf{r}_l)\, d\nu_k\, d\nu_l. \tag{21}$$

Finally, spatially correlated diffusion noise sources in (8) can be incorporated into the impedance field method formalism in (21) to calculate the noise voltage spectral densities at the gate and the drain.

III. Numerical Implementation

We describe a 3-D discretization and then a 2-D implementation with rectangular segments. The subscripts k and l now denote the k-th and l-th segments within the device, and $\mathbf{r}_k$ and $\mathbf{r}_l$ are the center points of each segment. We can thus modify (21) for the discretized problem as

$$\langle v_p v_q^* \rangle = \sum_k \sum_l \nabla G_{pk} \cdot \langle \mathbf{j}_k \mathbf{j}_l^* \rangle \cdot \nabla G_{ql}^*\, \Delta\nu_k \Delta\nu_l, \tag{22}$$

where the correlated diffusion noise source $\langle \mathbf{j}_k \mathbf{j}_l^* \rangle$ from (8) is

$$\langle \mathbf{j}_k \mathbf{j}_l^* \rangle = 4q^2 n_k \frac{1}{\Delta\nu_l} \mathbf{D}_{kl}(\omega). \tag{23}$$

In the discrete representation, n_k, $\mathbf{D}_{kl}$, ∇G_{pk}, and ∇G_{qk} are considered constant within each segment. If there is no spatial correlation of local velocity fluctuations between segments, i.e., if $\mathbf{D}_{kl}(\omega) = 0$ when $k \neq l$, we can rewrite (22) as

$$\langle v_p v_q^* \rangle = \sum_k 4q^2 n_k \nabla G_{pk} \cdot \mathbf{D}_{kk}(\omega) \cdot \nabla G_{qk}^* \, \Delta\nu_k. \tag{24}$$

In order to investigate the impact of the spatially correlated diffusion noise sources on the terminal noise, the Green's functions and the correlated (and uncorrelated) diffusion noise sources should be determined throughout the device and incorporated into (22) and (24) to compare the results.

By using the adjoint network approach [3] for which reciprocity holds between the linearized system (FET) and its adjoint, the impedance field G can be obtained by applying a unit current at the output terminal p or q in the adjoint network and finding the voltage produced at every internal node (mesh point), $\mathbf{r}_k$, instead of exciting the noise current for each of the segments in the original system and observing the voltage v_p or v_q produced at the terminal. This results in significant computational savings [3]. We used a commercial drift-diffusion device solver to obtain the Green's functions [20]. Subsequently, using MATLAB, the 2-D gradient of Green's function was calculated using finite differences.

The correlated diffusion noise source has been determined by Monte-Carlo simulation for homogeneous GaAs [7]. In our numerical noise study, the uncorrelated diffusion noise source was determined first, from which a representation for the correlated diffusion noise source was deduced. Within the domain of applicability of the drift-diffusion model, this approach allows implementation of a predetermined spatial correlation. This serves our purpose to evaluate the influence of spatial correlation. To implement the correct physical correlation would require, for example, a Monte Carlo solution of the actual device.

For the 2-D numerical device solution we employ, it is assumed that the Einstein relation holds, and that the uncorrelated diffusion noise source is isotropic (i.e., the tensor $\mathbf{D}$ is isotropic). Then, the diffusion coefficient D_k for the k-th segment is calculated from the electron mobility, $\mu_n(E)$, using the Einstein relation, assuming a lattice temperature T. With isotropic diffusivity, (24) can be rewritten as

$$\langle v_p v_q^* \rangle = \sum_k 4q^2 n_k D_k \, \nabla G_{pk} \cdot \nabla G_{qk}^* \, \Delta\nu_k, \tag{25}$$

where the scalar value of the noise source $4q^2 n_k D_k$ is multiplied with the dot (inner) product of the gradients of the Green's functions.

The uncorrelated diffusion noise source (i.e., $\langle \mathbf{j}_k \mathbf{j}_l \rangle = 0$ when $k \neq l$) assumes that the segment size is large enough (as shown in Fig. 1(a)) so that electrons perfectly lose the memory of their velocities because of the many scattering within a segment. However, as the device size shrinks, so does the segment size (as shown in Fig. 1(b)), and velocity fluctuations in nearby segments can be correlated. Comparing Figs. 1(a) and (b), we can assume that the velocity autocorrelation function for an electron spatially localized (in terms of correlation) within the large segment in Fig. 1(a) is equal to the summation of the cross-correlation functions over the nearby segments (small

dashed boxes) in Fig. 1(b). The implication is that there is an equivalent diffusion noise source that represents the superposition of a neighborhood of correlated diffusion noise sources, and in our work, that this equivalent noise source can be determined using a drift-diffusion model.

Consider a 1-D structure, which in our case is the 2DEG at the AlGaN/GaN interface. At the k-th segment, through superposition, the equivalent diffusion coefficient can be written in general in terms of a sum of cross-correlation terms as [7]

$$D_k = \sum_{l=1}^{L} D_{kl}, \tag{26}$$

where L is the number of segments (including the k-th segment) where spatial correlation persists from the k-th segment. Scatter diminishes correlation [7], so L defines a neighborhood. For example, if perfect correlation is assumed over a neighborhood comprised of segments within the mean-free path (l_s), from (26), $D_{kl} = D_k/L$. One could consider a symmetric neighborhood, and we take this view as an extreme case in evaluating the impact of spatial correlation on the terminal noise. If the channel distance variable is x and the segment length is Δx, then $L = 1 + I\{2l_s/\Delta x\}$, where $I\{\cdot\}$ is the integer value. Figure 2 illustrates the concept of how the spatially correlated diffusion noise source can be determined using this simple procedure. For example, if $\Delta x = 10$ nm and the correlation length l_s is 20 nm, electrons are assumed to travel (either left or right from the k-th segment in Fig. 2) without their velocity being randomized within l_s, and spatial correlation persists over 5 segments (including the k-th segment). Therefore, $D_{kl} = D_k/5$. A more sophisticated approach may involve using predetermined correlation calculations to ascribe weights that would diminish with distance. Also, the symmetry could be changed to account for the influence of the applied electric field, i.e., electron energy, on scatter [7].

In our numerical noise study using the example of an AlGaN/GaN HEMT, we focused on the noise contribution from the active channel region (the 2DEG). The 2-D numerical solver was used to obtain the parameters (i.e., n_k, D_k, G_{gk}, and G_{dk}) at all points within the device. Considering the 1-D channel only (similar to the one shown in Fig. 2), we determined the correlation terms D_{kl}, assuming (26), and evaluated their effect in calculating the terminal noise using the impedance field method. Note that (22) includes the 3-D gradients of the Green's functions and a tensor $\mathbf{D}_{kl}$. Because only the longitudinal segments along the 1-D channel are considered, we assume that $\mathbf{D}_{kl}$ has the (anisotropic) longitudinal diffusivity D_{kl} only for the correlated diffusion noise source. Therefore, with longitudinal diffusivity ($\hat{x}$ component) only, and applying (23) to (22) assuming $\omega = 0$,

$$\langle v_p v_q^* \rangle = \sum_k 4q^2 n_k \frac{\partial G_{pk}}{\partial x} \left(\sum_{l=1}^{L} D_{kl} \frac{\partial G_{ql}^*}{\partial x} \right) \Delta\nu_k, \tag{27}$$

where $\partial G_{gk}/\partial x$ and $\partial G_{dl}/\partial x$ were obtained from finite differences. As we will show from the numerical simulation, $|\partial G/\partial x| \gg |\partial G/\partial y|$ for the Green's functions involving both the gate and the drain. Thus, both the physical confinement of electrons to the channel and $|\partial G/\partial y|$ being small supports the 1-D representation for noise. The width dimension is assumed to be large relative to the (x, y) features, allowing a 2-D numerical simulation. The

influence of the correlated diffusion noise on the calculation of the intrinsic noise sources can be investigated by comparing the simulation results from (25) and (27).

IV. Noise Simulation

A. FET Geometry

The numerical device solver we employed allows the simulation of electrical behavior in a 2-D structure assuming a drift-diffusion model [20]. Figure 3 shows the 2-D device geometry of an $Al_{0.3}Ga_{0.7}N$/GaN HEMT used in the numerical simulation. The entire region was divided into a grid of mutually orthogonal lines, with solutions to be determined at each of the mesh points. In Fig. 3, the longitudinal grid spacing, Δx, is 10 nm. The vertical grid spacing, Δy, is 1 nm, but is gradually increasing below the channel. This device has a 0.25 μm gate length (from $x = 0$ to 0.25 μm in Fig. 3) and a 180 Å AlGaN barrier layer. The 2-D results are scaled for the gate width, 250 μm in this case, making this device consistent with one for which we have experimental noise data [18]. The gate-to-drain spacing (2.0 μm) is larger than the gate-to-source spacing (0.5 μm) to alleviate breakdown in the gate-to-drain junction at higher drain bias (the device was fabricated with a view to power applications) [11]. We consider the entire 2DEG region between source and drain metals (thus from $x = -0.5$ to 2.25 μm in Fig. 3) as the intrinsic transistor to be numerically characterized.

While doping is not necessary in the actual device fabrication due to spontaneous polarization and strain-induced piezoelectricity [11], the 2DEG region in the numerical model was intentionally doped to the required electron sheet density. The doping concentration, the AlGaN barrier thickness (18 nm), and field-dependent electron mobility model parameters were adjusted to match the measured DC I-V and AC (S-parameter) results.

We consider mesh points along the dashed line (y=19 nm) in Fig. 3 and the segments that enclose each node at their center point. Similarly, in numerical noise modeling for a short channel MOSFET using an uncorrelated diffusion noise source only, the 2-D problem was simplified to 1-D with the assumption that the inversion layer of the CMOS (active channel) is very thin [9].

B. Simulation Results

The noise simulation results presented are based on the Green's function approach described in the previous sections. First, the uncorrelated diffusion noise source and Green's functions at each node within the device (the 2DEG channel in the HEMT) were obtained by a 2-D numerical device solution. The gradients of the Green's functions were calculated by using MATLAB [21], and the correlated diffusion noise source was deduced from (26). Equations (25) and (27), incorporated into MATLAB, were used to calculate the noise voltage spectral densities at the gate and the drain terminals ($\langle|v_g|^2\rangle$, $\langle|v_d|^2\rangle$, and $\langle v_g v_d^*\rangle$). The spatially correlated diffusion noise source D_{kl} was employed in (27) to investigate the impact on the terminal noise calculation. Finally, we can transform $\langle|v_g|^2\rangle$, $\langle|v_d|^2\rangle$, and $\langle v_g v_d^*\rangle$ into the noise current spectral densities, $\langle|i_g|^2\rangle$, $\langle|i_d|^2\rangle$, and $\langle i_g i_d^*\rangle$ by using the defining relation between Y-parameters and Z-parameters [18], [22].

Figure 4 shows the simulated uncorrelated diffusion noise source along the channel, i.e., the dashed line (y=19 nm) in Fig. 3. The device is biased at V_{ds} = 4 V and I_{ds} = 60 mA, and f = 1 GHz. As this bias point is in the saturation region, the electron charge density (n) is depleted, which results in less diffusion noise ($4q^2n\ D$) right under the gate. Note that the ohmic regions (extrinsic elements) under the drain and source metal contacts are excluded from the noise calculation.

Figure 5 shows the Green's functions, $G_g(x)$ and $G_d(x)$, obtained from the 2-D device solution. Note that $\Im\{G_g\}$ and $\Im\{G_d\}$, the imaginary parts of G_g and G_d obtained at 1 GHz, are both negligible in comparison to the real parts $\Re\{G_g\}$ and $\Re\{G_d\}$. Also note that both $\Re\{G_g\}$ and $\Re\{G_d\}$ are varying rapidly in the channel region right under the gate metal ($x = 0 - 0.25\ \mu$m). Figure 6 shows the calculated gradients of the Green's functions. The results for $|\partial G_g/\partial x|$ and $|\partial G_g/\partial y|$, and also $|\partial G_d/\partial x|$ and $|\partial G_d/\partial y|$, are plotted on a logarithmic magnitude scale to more clearly show the differences. Note that $|\partial G_g/\partial x| \gg |\partial G_g/\partial y|$ and $|\partial G_d/\partial x| \gg |\partial G_d/\partial y|$, indicating that the longitudinal variation of the Green's function dominates. As shown in Figs. 5 and 6, the gradient of the Green's functions under the gate-to-source region dominates, and the gradient of the drain Green's function is an order of magnitude larger than that for the gate.

We use the Green's function approach to calculate the gate and drain terminal noise sources. Figure 7 shows the calculated contribution of the local diffusion noise source (uncorrelated and correlated) at the gate and drain terminals. The solid lines are the cases where an uncorrelated diffusion noise source is used for the gate and drain ($4q^2n_kD_k|\nabla G_{gk}|^2$ and $4q^2n_kD_k|\nabla G_{dk}|^2$, from (25)). To investigate the impact of correlation, different correlation lengths l_s (10-50 nm) were chosen for simulation, based on the evaluation of mean-free path (average electron velocity divided by the scattering rate) estimated for an AlGaN/GaN 2DEG [23], [24]. The long dashed lines in Fig. 7 are the case where there is perfect correlation over the length of $\pm$30 nm, i.e., l_s = 30 nm, and $D_{kl} = D_k/7$. Beyond 30 nm, the spatial correlation between local fluctuations is assumed to vanish. Thus, referring to (27), the dashed lines in Figs. 7(a) and (b) were determined from $4q^2n_k\frac{D_k}{L}(\frac{\partial G_{gk}}{\partial x})\sum \frac{\partial G^*_{gl}}{\partial x}$ and $4q^2n_k\frac{D_k}{L}(\frac{\partial G_{dk}}{\partial x})\sum \frac{\partial G^*_{dl}}{\partial x}$. Figure 7 shows that the noise contribution of the correlated diffusion noise source to the gate and drain terminal is different from the case where the uncorrelated diffusion noise source is used (solid lines). This difference is pronounced under the gate (the gate metal covers from x = 0 to 0.25 μm). This is because the diffusion noise source is multiplied with the gradient of the Green's functions, which vary appreciably in the channel region under the gate, as shown in Fig. 6. Also note in Fig. 7 that both the gate noise and the drain noise result mostly from the gate-to-source region and under the gate in the channel. A similar trend was found in a CMOS device studied [9]. While the local diffusion noise source is small under the gate due to the charge depletion (see Fig. 4), this noise source is multiplied by large Green's function gradients and thus results in an appreciable noise contribution at the gate and drain.

C. Intrinsic FET Noise Sources

In the simple FET equivalent-circuit model, one can generally anticipate correlation between the gate and drain noise current by capacitive (C_{gs}) coupling [18]. For example, i_d induces the gate voltage v_g through the transconductance, g_m. Then, $v_g = i_d/g_m$ if perfect correlation can be assumed, and $i_g = j\omega C_{gs} v_g = j\omega C_{gs} i_d/g_m$. This produces a noise variance of $\langle |i_g|^2 \rangle = \omega^2 C_{gs}^2 \langle |i_d|^2 \rangle / g_m^2$. We have demonstrated experimentally that, in the case of velocity fluctuation, $\langle |i_d|^2 \rangle$ is independent of frequency in the microwave operating range of the transistor (white noise), and hence $\langle |i_g|^2 \rangle \propto \omega^2$, thus establishing the concept of capacitive coupling between the gate and drain noise [18]. In order to assess the effect of the correlation between i_g and i_d, the correlation coefficient, C, is defined in normalized form as [18], [25]

$$C = \frac{\langle i_g i_d^* \rangle}{\sqrt{\langle |i_g|^2 \rangle \langle |i_d|^2 \rangle}}. \tag{28}$$

With perfect correlation assumed in the ideal noise model, $C = j1$.

Figures 8 and 9 show the simulated $\langle |i_g|^2 \rangle$, $\langle |i_d|^2 \rangle$, and the correlation coefficient C (magnitude and phase), transformed from $\langle |v_g|^2 \rangle$, $\langle |v_d|^2 \rangle$, and $\langle v_g v_d^* \rangle$ that are obtained by (25) and (27). We compare these results with those extracted from a noise measurement of the 0.25×250 μm^2 $Al_{0.3}Ga_{0.7}N$/GaN HEMT [18]. Both measurements and simulations result from velocity fluctuation only, with the influence of shot, $1/f$, and extrinsic thermal noise deembedded [18]. The drain noise simulation almost precisely matches the experimental result. The discrepancy in the gate noise result is due to the Schottky contact attributes not being correctly implemented in the numerical device solver [20]. We also noticed that the gate Green's function was sensitive to the AlGaN barrier layer thickness (nominally 20 nm), which might be different from that in the actual device fabricated. The correlation coefficient trend is also captured in the simulation result of Fig. 9. Using the diffusion noise source without correlation and assuming perfect correlation over up to 30 nm produce virtually the same noise results. This occurs because the noise sources, multiplied with the gradients of the Green's functions, are integrated over space, which tends to wash out the features evident in Fig. 7. Note in Figs. 8 and 9 that assuming perfect spatial correlation over l_s = 50 nm for the diffusion noise source generates slightly different results for the terminal noise (especially $\langle |i_d|^2 \rangle$ and $|C|$). However, it is our understanding that 50 nm is several mean-free paths, and thus electron velocities should be randomized after traveling such distance.

With the validated drift-diffusion noise model, Fig. 10 shows the simulated $\langle |i_d|^2 \rangle$ for different bias conditions. Note that $\langle |i_d|^2 \rangle$ increases with I_{ds}, but does not change appreciably with V_{ds} in the saturation regime, as shown in Fig. 10. This observation is consistent with those from our measurements [18]. The current-dependent noise arises from non-equilibrium transport in the channel, with both noise sources and Green's functions being a function of bias.

To first order, high channel mobility and high unity current gain frequency f_T produce low velocity fluctuation noise. The 2DEG mobility for an AlGaN/GaN HEMT has been measured to be 1500 cm^2/V-sec at 300 K and 7900 cm^2/V-sec at 80 K [12]. The device we made measurements on had f_T = 40 GHz. The noise in this relatively

high-speed device is modeled quite nicely using a drift-diffusion model.

V. Conclusion

Numerical noise modeling allows interrogation of intrinsic properties that contribute to measured terminal noise. While Monte Carlo techniques provide a more rigorous physical model, the simple drift-diffusion model used predicts the velocity fluctuation noise in the 0.25 μm AlGaN/GaN HEMT studied. The correlation of the diffusion noise source over meaningful lengths did not alter the terminal noise significantly, leading to the conclusion that an uncorrelated model is sufficient. One would expect that for yet smaller device geometries noise source correlation would become more important. Such smaller-scale devices may require a Boltzmann transport equation model. It is possible that there is a regime where a drift-diffusion noise model is applicable and correlation is important, making the simple neighborhood correlation concept introduced an expedient tool. While the numerical implementation described involved a drift-diffusion model to determine both the noise sources and the Green's functions, the concept of noise sources based on velocity fluctuations is general, as is the notion of a neighborhood correlation scheme.

VI. Acknowledgment

The authors would like to thank Dr. J. Sanchez of Synopsys for helpful discussions concerning the use of the Taurus Device, numerical device solver. This work was supported by AFOSR under contract F49620-03-1-0405 and ONR under contracts N00014-98-1-0371 and N00014-99-C-0172.

References

[1] W. Shockley, J. A. Copeland, and R. P. James, "The impedance field method of noise calculation in active semiconductor devices," in *Quantum Theory of Atoms, Molecules, and the Solid State*, 1966, pp. 537–563, New York: Academic Press.

[2] A. Cappy, "Noise modeling and measurement techniques," *IEEE Trans. Microwave Theory Tech.*, vol. 36, no. 1, pp. 1–10, Jan. 1988.

[3] F. Bonani and G. Ghione, *Noise in Semiconductor Devices*, Springer-Verlag, 2001.

[4] J. P. Nougier, "Fluctuations and noise of hot carriers in semiconductor materials and devices," *IEEE Trans. Electron Dev.*, vol. 41, no. 11, pp. 2034–2048, Nov. 1994.

[5] P. Shiktorov, E. Starikov, V. Gruzinskis, T. Gonzalez, J. Mateos, D. Pardo, L. Reggiani, L. Varani, and J. C. Vaissiere, "Langevin forces and generalized transfer fields for noise modeling in deep submicron devices," *IEEE Trans. Electron Dev.*, vol. 47, no. 10, pp. 1992–1998, Oct. 2000.

[6] J. P. Nougier, J. C. Vaissiere, and C. Gontrand, "Two-point correlations of diffusion noise sources of hot carriers in semiconductors," *Phys. Rev. Lett.*, vol. 51, no. 6, pp. 513–516, Aug. 1983.

[7] J. Mateos, T. Gonzalez, and D. Pardo, "Spatial extent of the correlations between local diffusion noise sources in GaAs," *J. Appl. Phys.*, vol. 77, no. 4, pp. 1564–1568, Feb. 1995.

[8] J. Mateos, T. Gonzalez, and D. Pardo, "Influence of spatial correlations on the analysis of diffusion noise in submicron semiconductor structures," *Appl. Phys. Lett.*, vol. 67, no. 5, pp. 685–687, July 1995.

[9] J. S. Goo, C. H. Choi, F. Danneville, E. Morifuji, H. S. Momose, Z. Yu, H. Iwai, T. H. Lee, and R. W. Dutton, "An accurate and efficient high frequency noise simulation technique for deep submicron MOSFETs," *IEEE Trans. Electron Devices*, vol. 47, no. 12, pp. 2410–2419, Dec. 2000.

[10] S. Lee and K. J. Webb, "Numerical noise model for the AlGaN/GaN HEMT," in *2004 IEEE MTT-S Int. Microwave Symp. Dig.*, June 2004, vol. 2, pp. 1055–1058, Fort Worth, TX.

[11] L. F. Eastman, V. Tilak, J. Smart, B. M. Green, E. M. Chumbes, R. Dimitrov, H. Kim, O. S. Ambacher, N. Weimann, T. Prunty, M. Murphy, W. J. Schaff, and J. R. Shealy, "Undoped AlGaN/GaN HEMTs for microwave power amplification," *IEEE Trans. Electron Devices*, vol. 48, no. 3, pp. 479–485, Mar. 2001.

[12] P. B. Shah, D. D. Smith, T. E. Griffin, K. A. Jones, and S. T. Sheppard, "Carrier transport related analysis of high-power AlGaN/GaN HEMT structures," *IEEE Trans. Electron Devices*, vol. 47, no. 3, pp. 308–312, Feb. 2000.

[13] W. B. Davenport and W. L. Root, *An Introduction to the Theory of Random Signals and Noise*, McGraw-Hill, 1958.

[14] *Physics of Nonlinear Transport in Semiconductors*, New York: Plenum, 1980, edited by D. K. Ferry, J. R. Barker, C. Jacoboni.

[15] A. Einstein, "Uber die von der molekularkinetischen theorie der warme geforderte bewegung von in ruhenden flussigkeiten suspendierten teilchen (on the motion, required by the molecular kinetic theory of heat, of small particles suspended in a stationary liquid)," *Ann. d. Phyz.*, vol. 17, pp. 549–560, 1905.

[16] H. Nyquist, "Thermal agitation of electric charge in conductors," *Phys. Rev.*, vol. 32, pp. 110–113, July 1928.

[17] M. W. Pospieszalski, "Modeling of noise paramters of MESFET's and MODFET's and their frequency and temperature dependence," *IEEE Trans. Microwave Theory Tech.*, vol. 36, no. 1, pp. 1–10, Jan. 1988.

[18] S. Lee, K. J. Webb, V. Tilak, and L. F. Eastman, "Intrinsic noise equivalent circuit parameters for AlGaN/GaN HEMTs," *IEEE Trans. Microwave Theory Tech.*, vol. 51, no. 5, pp. 1567–1577, May 2003.

[19] F. Bonani, G. Ghione, M. R. Pinto, and R. K. Smith, "An efficient approach to noise analysis through multidimensional physics-based models," *IEEE Trans. Electron Dev.*, vol. 45, no. 1, pp. 261–269, Jan. 1998.

[20] Synopsys, *Taurus-Device User Guide*, Version 2003.12.

[21] MathWorks, *MATLAB User Guide*, Version 6.5.1.

[22] H. Hillbrand and P. H. Russer, "An efficient method for computer aided noise analysis of linear amplifier networks," *IEEE Trans. on Circuit Syst.*, vol. 23, no. 4, pp. 235–238, Apr. 1976.

[23] B. E. Foutz, S. K. O'Leary, M. S. Shur, and L. F. Eastman, "Electron transport in the III-V nitride alloys," in *Materials Research Society Symposium Proceedings*, 1999, vol. 572, pp. 501–506.

[24] L. F. Eastman, A. Matulionis, and A. Vertiatchikh, "Scattering limitations on electron transit velocity in AlGaN/GaN HEMTs," in *Proc. Int. Symp. Compound Semicond.*, 2003, pp. 167–168.

[25] H. Statz, H. A. Haus, and R. A. Pucel, "Noise characteristics of gallium arsenide field-effect transistors," *IEEE Trans. Electron Devices*, vol. 21, pp. 549–562, Sep. 1974.

Figure Captions

Fig. 1. (a) A large segment (dashed box) for which the uncorrelated diffusion noise source may be an adequate representation. (b) Smaller segments where the electron velocity fluctuations between segments (smaller square dashed boxes) are spatially correlated.

Fig. 2. Discretized 1-D structure. The diffusion noise source for the k-th segment has noise contributions over neighboring segments, with their cross-correlation terms (denoted as D_{kl}) dependent on how long the correlation length is.

Fig. 3. AlGaN/GaN HEMT device geometry used in the numerical simulation. The longitudinal (along with the channel) and vertical grid spacings are represented as Δx and Δy, respectively. The gate length is 0.25 μm.

Fig. 4. Simulated local (uncorrelated) diffusion noise source along the 2DEG channel for the AlGaN/GaN HEMT. The device is biased at V_{ds} = 4 V, I_{ds} = 60 mA. f = 1 GHz. The AlGaN/GaN HEMT has 0.25 μm gate length (from $x = 0$ to 0.25 μm).

Fig. 5. Simulated Green's function (impedance field) for (a) the gate and (b) the drain. The device is biased at V_{ds} = 4 V, I_{ds} = 60 mA, and f = 1 GHz. The complex Green's function has units Ω, and $\Re\{\ \}$ and $\Im\{\ \}$ are the real and imaginary parts.

Fig. 6. Calculated magnitude of the gradient of the complex Green's function (impedance field) for (a) the gate and (b) the drain. The device is biased at V_{ds} = 4 V, I_{ds} = 60 mA, and f = 1 GHz.

Fig. 7. The contribution of the local diffusion noise source (noise source multiplied with the gradient of the Green's function and its conjugate) to (a) the gate and (b) the drain noise. The device is biased at V_{ds} = 4 V, I_{ds} = 60 mA, and f = 1 GHz.

Fig. 8. Simulated (a) $\langle |i_g|^2 \rangle$ and (b) $\langle |i_d|^2 \rangle$. The device is biased at V_{ds} = 4 V, I_{ds} = 60 mA. The symbol (x) is the measurement result (velocity fluctuation only, after deembedding shot and $1/f$ noise) from the 0.25×250 μm^2 AlGaN/GaN HEMT.

Fig. 9. (a) The magnitude and (b) phase of the simulated correlation coefficient. The device is biased at V_{ds} = 4 V, I_{ds} = 60 mA. The symbol (x) is the measurement result (velocity fluctuation only, after deembedding shot and $1/f$ noise) from the 0.25×250 μm^2 AlGaN/GaN HEMT.

Fig. 10. Simulated $\langle |i_d|^2 \rangle$ (velocity fluctuation only). The device is biased at I_{ds} = 30, 60, 90 mA, and for I_{ds} = 60 mA, V_{ds} = 4, 6, 8 V.

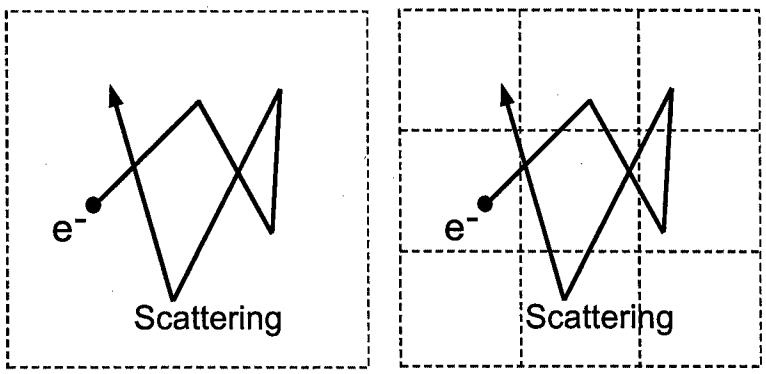

(a) (b)

Fig. 1.

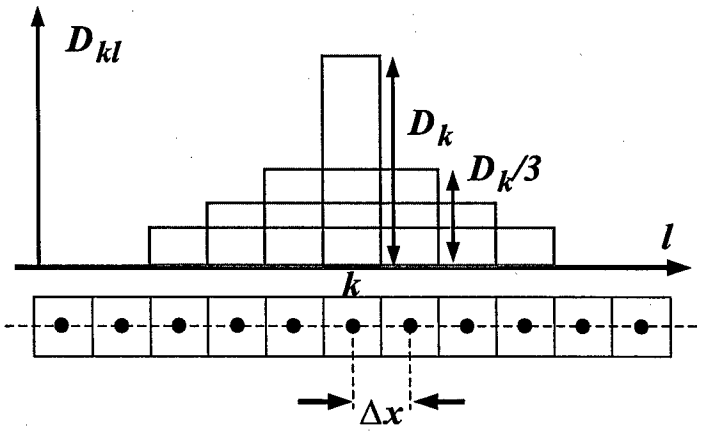

Fig. 2.

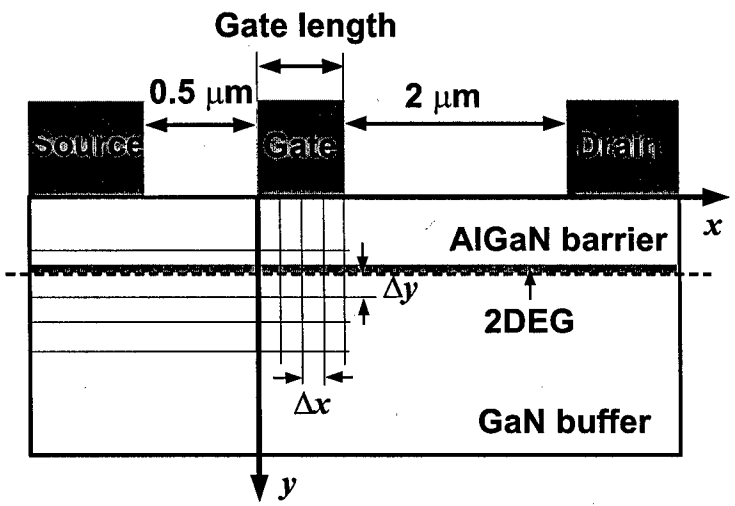
Gate length
0.5 μm
2 μm
Source
Gate
Drain
x
AlGaN barrier
Δy
2DEG
Δx
GaN buffer
y

Fig. 3.

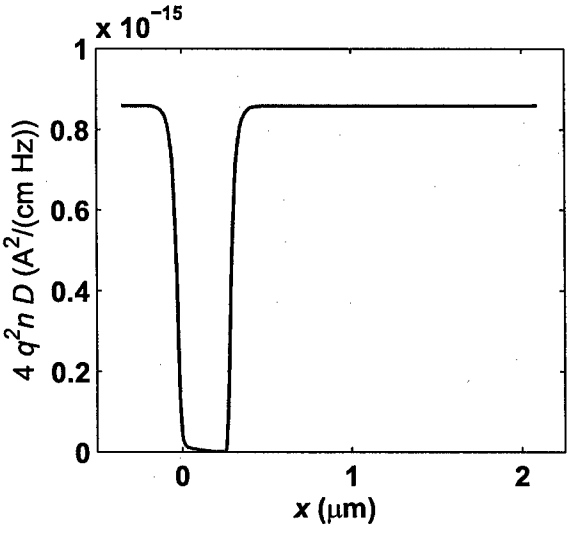

Fig. 4.

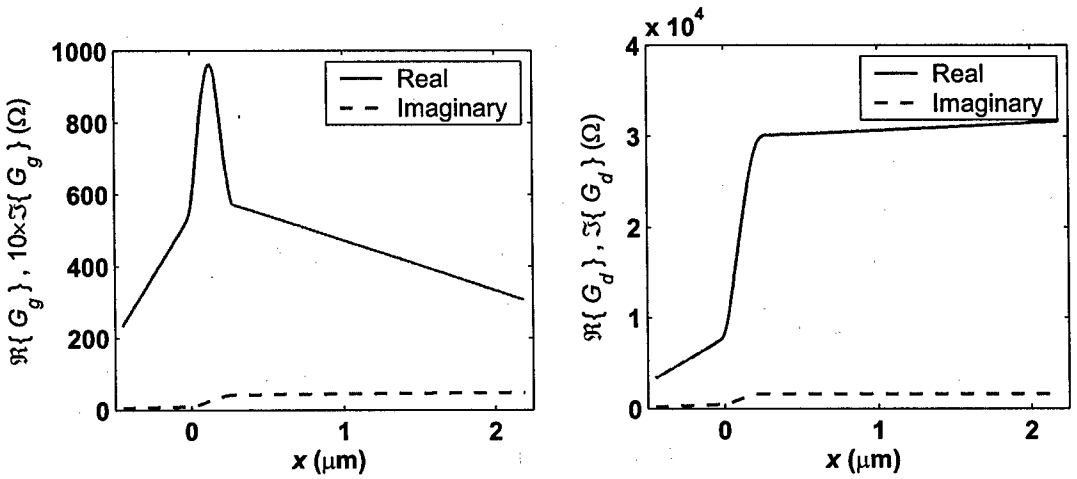
1000
800
600
400
200
0
0
1
2
x (μm)
ℜ{ G_g }, 10×ℑ{ G_g } (Ω)
Real
Imaginary
x 10^4
4
3
2
1
0
0
1
2
x (μm)
ℜ{ G_d }, ℑ{ G_d } (Ω)
Real
Imaginary

(a) (b)

Fig. 5.

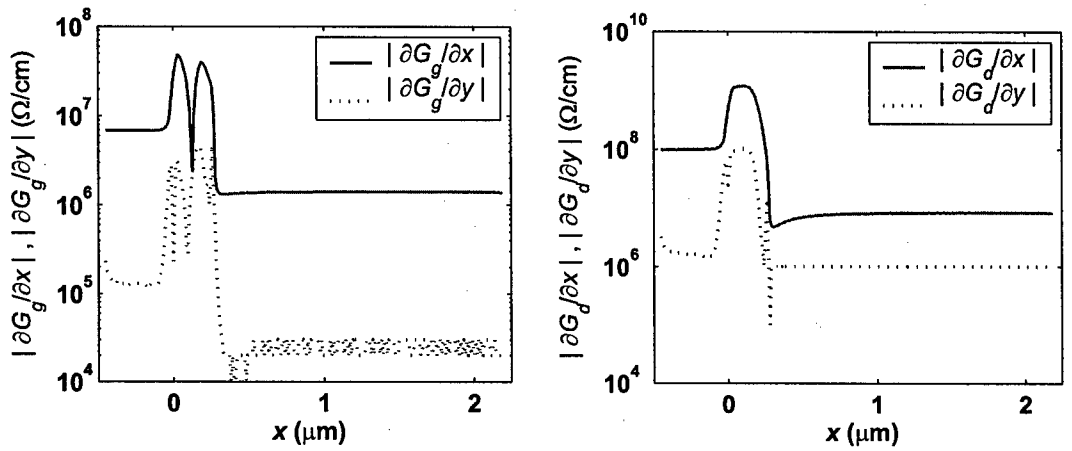
10^8
10^7
10^6
10^5
10^4
$|\partial G_g/\partial x|$, $|\partial G_g/\partial y|$ (Ω/cm)
$|\partial G_g/\partial x|$
$|\partial G_g/\partial y|$
0
1
2
x (μm)
10^{10}
10^8
10^6
10^4
$|\partial G_d/\partial x|$, $|\partial G_d/\partial y|$ (Ω/cm)
$|\partial G_d/\partial x|$
$|\partial G_d/\partial y|$
0
1
2
x (μm)

(a) (b)

Fig. 6.

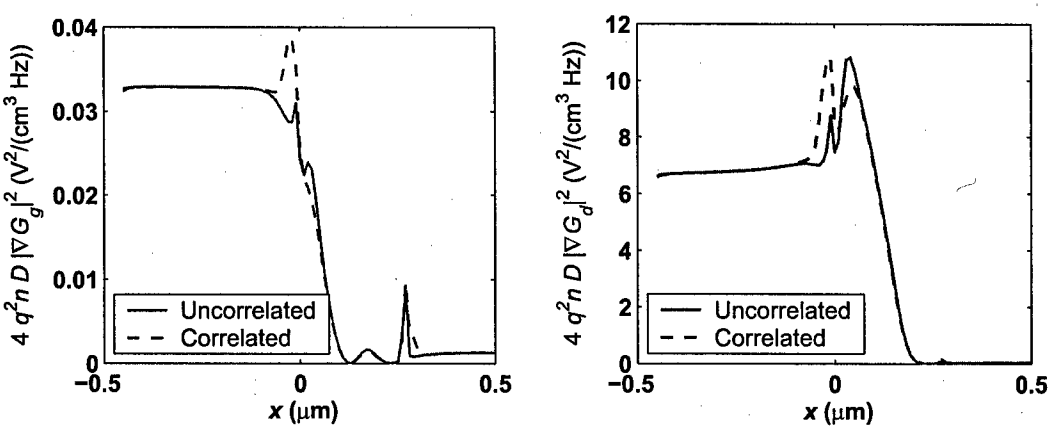
0.04
0.03
0.02
0.01
0
−0.5
0
0.5
x (μm)
4 q²n D |∇G_g|² (V²/(cm³ Hz))
Uncorrelated
Correlated
12
10
8
6
4
2
0
−0.5
0
0.5
x (μm)
4 q²n D |∇G_d|² (V²/(cm³ Hz))
Uncorrelated
Correlated

(a) (b)

Fig. 7.

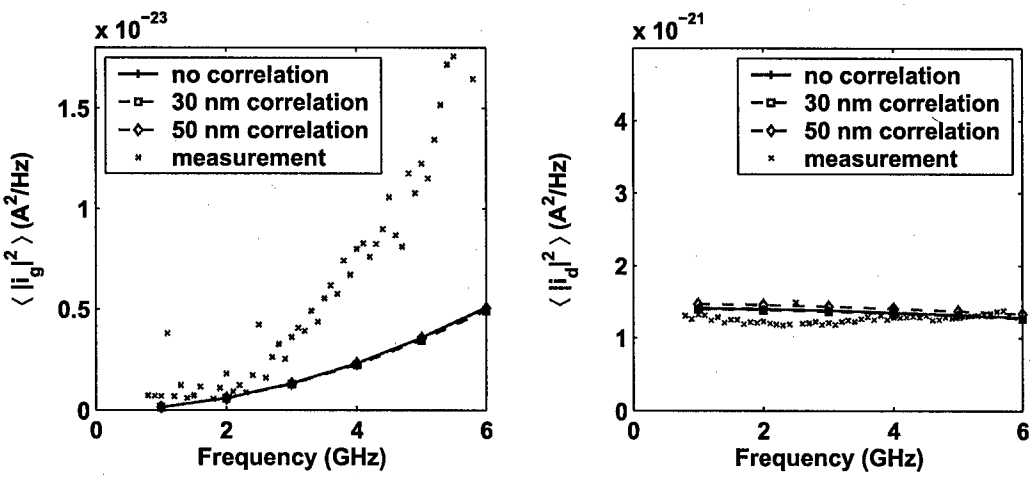
x 10^-23
no correlation
30 nm correlation
50 nm correlation
measurement
⟨|i_g|^2⟩ (A^2/Hz)
Frequency (GHz)
x 10^-21
no correlation
30 nm correlation
50 nm correlation
measurement
⟨|i_d|^2⟩ (A^2/Hz)
Frequency (GHz)

(a) (b)

Fig. 8.

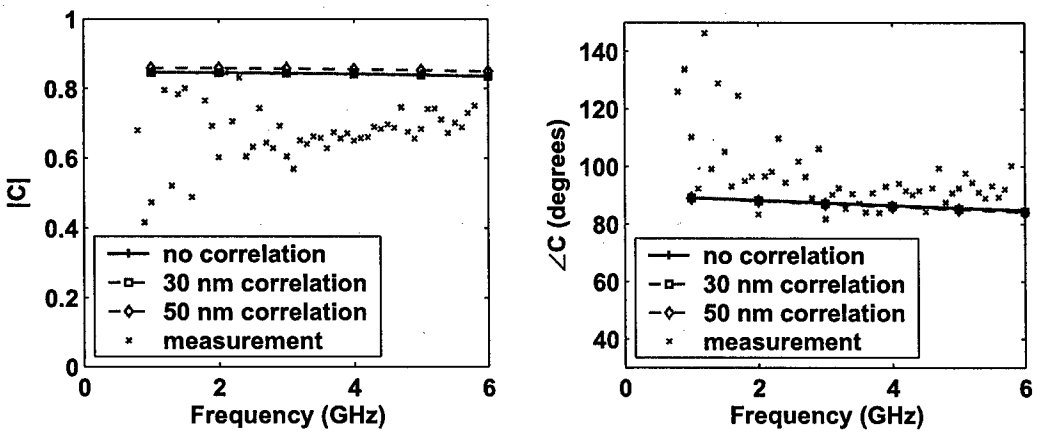
|C|
Frequency (GHz)
no correlation
30 nm correlation
50 nm correlation
measurement
∠C (degrees)
Frequency (GHz)
no correlation
30 nm correlation
50 nm correlation
measurement

(a) (b)

Fig. 9.

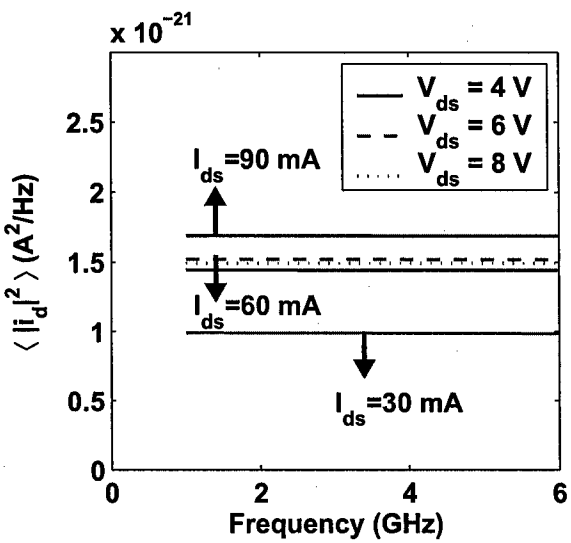
x 10^-21
2.5
2
1.5
1
0.5
0
0
2
4
6
Frequency (GHz)
⟨|i_d|^2⟩ (A^2/Hz)
V_ds = 4 V
V_ds = 6 V
V_ds = 8 V
I_ds=90 mA
I_ds=60 mA
I_ds=30 mA

Fig. 10.